

Complexity and efficiency of minimum entropy production probability paths from quantum dynamical evolutions

Carlo Cafaro,¹ Shannon Ray,² and Paul M. Alsing²¹*SUNY Polytechnic Institute, Albany, New York 12203, USA*²*Air Force Research Laboratory, Information Directorate, Rome, New York 13441, USA*

(Received 23 July 2021; accepted 11 March 2022; published 31 March 2022)

We present an information geometric characterization of quantum driving schemes specified by $su(2; \mathbb{C})$ time-dependent Hamiltonians in terms of both complexity and efficiency concepts. Specifically, starting from pure output quantum states describing the evolution of a spin-1/2 particle in an external time-dependent magnetic field, we consider the probability paths emerging from the parametrized squared probability amplitudes of quantum origin. The information manifold of such paths is equipped with a Riemannian metrization specified by the Fisher information evaluated along the parametrized squared probability amplitudes. By employing a minimum action principle, the optimum path connecting initial and final states on the manifold in finite time is the geodesic path between the two states. In particular, the total entropy production that occurs during the transfer is minimized along these optimum paths. For each optimum path that emerges from the given quantum driving scheme, we evaluate the so-called information geometric complexity (IGC) and our newly proposed measure of entropic efficiency constructed in terms of the constant entropy production rates that specify the entropy minimizing paths being compared. From our analytical estimates of complexity and efficiency, we provide a relative ranking among the driving schemes being investigated. Moreover, we determine that the efficiency and the temporal rate of change of the IGC are monotonic decreasing and increasing functions, respectively, of the constant entropic speed along these optimum paths. Then, after discussing the connection between thermodynamic length and IGC in the physical scenarios being analyzed, we briefly examine the link between IGC and entropy production rate. Finally, we conclude by commenting on the fact that a higher entropic speed in quantum transfer processes seems to necessarily go along with a lower entropic efficiency together with a higher information geometric complexity.

DOI: [10.1103/PhysRevE.105.034143](https://doi.org/10.1103/PhysRevE.105.034143)

I. INTRODUCTION

The goodness of an algorithm can be assessed by a variety of criteria [1]. In general, to quantify the performance of algorithms in both classical and quantum settings, one considers the asymptotic scaling of a complexity measure such as runtime or space usage with problem size [2]. Runtime is measured by the number of elementary operations employed by the algorithm. In particular, being in the framework of quantum computing [3], runtime can be specified in terms of the number of quantum gates applied to qubits in a quantum circuit model [4]. In general, when ranking the performances of various algorithms that solve the same task, one usually considers the asymptotic behavior in the problem size of the time or space complexity of the algorithm. The choice of focusing on the asymptotic behavior is dictated by the fact that for small input sizes, almost any algorithm can be sufficiently efficient. Addressing questions concerning the computational performance of algorithms can be rather tricky. For instance, specifying how long it takes for the algorithm to produce the desired output or how much memory it needs to generate it can depend on a number of factors, including the speed of the computer, the programming language, the efficiency of the implementation, and the value of the input. What does

“efficient” mean, exactly? Do efficient algorithms exhibit a lower degree of complexity? Which type of complexity are we referring to? A partial list of complexity measures we may be making reference to includes conceptual complexity, computational complexity, space complexity, and time complexity. It is possible to propose efficiency measures that capture different aspects of the algorithm. For instance, Traub’s efficiency index $\eta_{\text{Traub}} \stackrel{\text{def}}{=} p/\epsilon$ is an asymptotic estimate of the efficiency of an iterative method for computing a simple real root of an n th degree polynomial. This index depends on the order p of convergence to the solution and on the complexity parameter ϵ denoting the number of function evaluations per iteration. Clearly, one may think of proposing alternative efficiency measures, including one that takes into account the number of logical operations performed during the algorithm as proposed by Kung and Traub in Ref. [5]. For an overview of different efficiency measures for distinct iterative methods, we refer to Ref. [1].

In recent years, numerous investigations have been carried out with the goal of providing physical insights from Riemannian geometric characterizations [6–8] of thermodynamical concepts such as entropy production and efficiency [9–12]. In Ref. [9], using the notions of thermodynamic

length, thermodynamic divergence, and entropy production rate, the authors obtained geometric lower bounds on the entropy production in reversible quantum Markovian systems specified by master equations. In Ref. [10], making extensive use of thermodynamic geometry [7], the authors presented a general technique for optimizing the thermodynamic efficiency in microscopic quantum heat engines working close to equilibrium. In Ref. [11], employing solely thermodynamic geometry arguments, the authors found a universal tradeoff between efficiency and power for microscopic quantum heat engines driven by arbitrary periodic temperature changes. In Ref. [12], relying heavily on information geometric techniques [6], the authors proposed an information geometric interpretation of the entropy production for a total system and the partial entropy productions for subsystems. Furthermore, spin models were used in Ref. [12] to explain in an analytical fashion these physical findings of information geometric origin.

In this paper, building upon our previous results reported in Refs. [13–15] and inspired by the findings uncovered in Refs. [9–12], we provide a quantitative link between the concepts of *information geometric complexity* and *entropic efficiency* by studying the entropic dynamics on information manifolds emerging from exactly solvable time-dependent two-level quantum systems that mimic quantum search Hamiltonians. Our motivation for considering this type of work can be explained by pointing out a number of previous results our proposed analysis relies on. First, there is our previous investigation carried out in Ref. [16] concerning the physical connection between quantum search Hamiltonians and exactly solvable time-dependent two-level quantum systems [17,18]. Second, there are our previous attempts in trying to provide an information geometric perspective on the characterization of tradeoffs between speed and thermodynamic efficiency in quantum search algorithms [13–15]. Unfortunately, despite the agreement on the importance that quantum algorithms should be fast and thermodynamically efficient [19], there does not exist, to the best of our knowledge, any unifying theoretical description on this matter. Our work here aims at being a nontrivial step forward in this direction.

We provide an information geometric analysis of quantum driving schemes characterized by $\mathfrak{su}(2; \mathbb{C})$ time-dependent Hamiltonians by means of both complexity and efficiency concepts. From the knowledge of the pure output quantum states specifying the evolution of a spin-1/2 particle in an external magnetic field, we construct the probability paths emerging from the parametrized squared probability amplitudes. The Fisher information evaluated along the parametrized squared probability amplitudes provides a Riemannian metrization for such information manifolds. Imposing a minimum action principle, it happens that the optimum path connecting initial and final states on the manifold in finite time is the geodesic path between the two states. In particular, the total entropy production that occurs during the quantum transfer is minimized along these optimum paths. For each optimum path that arises from the given quantum driving Hamiltonian, we compute the so-called information geometric complexity (IGC) and our newly proposed measure of entropic efficiency. The latter quantity is expressed in terms of the constant entropy production rates that characterize the

entropy minimizing paths being examined. From our calculations of complexity and efficiency, we give a relative ranking among the driving schemes being compared. Moreover, we show that the efficiency and the temporal rate of change of the IGC are monotonic decreasing and increasing functions, respectively, of the constant entropic speed along these optimum paths. Then, after elaborating on the connection between thermodynamic length and IGC, we briefly discuss the relation between IGC and entropy production rate. Finally, we conclude by providing some remarks on the fact that an higher entropic speed in quantum transfer processes appears to necessarily lead to a lower entropic efficiency together with a higher IGC.

The layout of the remainder of this paper is as follows. In Sec. II, we present the IGC concept. In Sec. III, after introducing the concepts of thermodynamic length and thermodynamic divergence, we propose our measure of entropic efficiency. In Sec. IV, we describe the quantum driving schemes being studied and explain how to generate probability paths from the output quantum pure state emerging from the quantum mechanical evolution. Then, having identified the elapsed time as the key statistical parameter [20], we apply our proposed information geometric theoretical construct to four distinct quantum mechanical driving scenarios in Sec. V. Our final remarks appear in Sec. VI. Finally, technical details are located in Appendices A, B, C, and D.

II. INFORMATION GEOMETRIC COMPLEXITY

In this section, we introduce the concepts of information geometric entropy (IGE) and IGC.

The IGE is a measure of complexity that was originally introduced in Ref. [21] in the context of the information geometric approach to chaos (IGAC) theoretical setting developed in Ref. [22]. For brevity and readability of the paper, we do not mention any superfluous detail on the IGAC. However, for the interested reader we suggest considering the concise discussion on the IGAC in Ref. [23]. In what follows, we present the concept of IGE.

Suppose that the points $\{p(x; \theta)\}$ of an n -dimensional curved statistical manifold \mathcal{M}_s are parametrized in terms of n real valued variables $(\theta^1, \dots, \theta^n)$, where

$$\mathcal{M}_s \stackrel{\text{def}}{=} \{p(x; \theta) : \theta = (\theta^1, \dots, \theta^n) \in \mathcal{D}_\theta^{\text{tot}}\}. \quad (1)$$

The microvariables x belong to the microspace \mathcal{X} , while the macrovariables θ are elements of the parameter space $\mathcal{D}_\theta^{\text{tot}}$ defined as

$$\mathcal{D}_\theta^{\text{tot}} \stackrel{\text{def}}{=} (\mathcal{I}_{\theta^1} \otimes \mathcal{I}_{\theta^2} \dots \otimes \mathcal{I}_{\theta^n}) \subseteq \mathbb{R}^n. \quad (2)$$

The quantity \mathcal{I}_{θ^j} in $\mathcal{D}_\theta^{\text{tot}}$ is a subset of \mathbb{R}^n and specifies the range of allowable values for the statistical macrovariables θ^j . The IGE is proposed as a measure of temporal complexity of geodesic paths within the IGAC. The IGE is defined as

$$\mathcal{S}_{\mathcal{M}_s}(\tau) \stackrel{\text{def}}{=} \log \widetilde{\text{vol}}[\mathcal{D}_\theta(\tau)], \quad (3)$$

where the average dynamical statistical volume $\widetilde{\text{vol}}[\mathcal{D}_\theta(\tau)]$ is

$$\widetilde{\text{vol}}[\mathcal{D}_\theta(\tau)] \stackrel{\text{def}}{=} \frac{1}{\tau} \int_0^\tau \text{vol}[\mathcal{D}_\theta(\tau')] d\tau'. \quad (4)$$

We emphasize that $\mathcal{D}_\theta(\tau')$ in Eq. (4) is an n -dimensional subspace of $\mathcal{D}_\theta^{\text{tot}} \subseteq \mathbb{R}^n$ whose elements $\{\theta\}$ with $\theta = (\theta^1, \dots, \theta^n)$ are such that $\theta^j(\tau_0) \leq \theta^j \leq \theta^j(\tau_0 + \tau')$ with τ_0 being the initial value assumed by the affine parameter that specifies the geodesic paths as will be explained in more detail shortly. Observe that the operation of temporal average is denoted with the tilde symbol in Eq. (4). For clarity, we underline the fact that $\text{vol}[\mathcal{D}_\theta(\tau)]$ in Eq. (4) is defined in terms of two sequential integration procedures. A first integration occurs on the explored parameter space and yields $\text{vol}[\mathcal{D}_\theta(\tau')]$. Then, as second integration specifying a temporal averaging procedure is performed over the duration of the process and leads ultimately to $\text{vol}[\mathcal{D}_\theta(\tau)]$. Moreover, the volume $\text{vol}[\mathcal{D}_\theta(\tau')]$ in the right-hand side of Eq. (4) specifies the volume of an extended region on the manifold \mathcal{M}_s . It is defined as

$$\text{vol}[\mathcal{D}_\theta(\tau')] \stackrel{\text{def}}{=} \int_{\mathcal{D}_\theta(\tau')} \rho(\theta^1, \dots, \theta^n) d^n \theta. \quad (5)$$

The quantity $\rho(\theta^1, \dots, \theta^n) \stackrel{\text{def}}{=} \sqrt{g(\theta)}$ is the so-called Fisher density and is equal to the square root of the determinant $g(\theta)$ of the Fisher-Rao information metric tensor $g_{ij}(\theta)$, $g(\theta) \stackrel{\text{def}}{=} \det[g_{ij}(\theta)]$. The quantity $g_{ij}(\theta)$ is given by

$$g_{ij}(\theta) \stackrel{\text{def}}{=} \int p(x|\theta) \partial_i \log p(x|\theta) \partial_j \log p(x|\theta) dx, \quad (6)$$

with $\partial_i \stackrel{\text{def}}{=} \partial/\partial \theta^i$. The expression of $\text{vol}[\mathcal{D}_\theta(\tau')]$ in Eq. (5) becomes more transparent for manifolds with information metric tensor whose determinant can be factorized as

$$g(\theta) = g(\theta^1, \dots, \theta^n) = \prod_{j=1}^n g_j(\theta^j). \quad (7)$$

In this case, the IGE in Eq. (3) can be recast as

$$\begin{aligned} \mathcal{S}_{\mathcal{M}_s}(\tau) \\ = \log \left\{ \frac{1}{\tau} \int_0^\tau \left[\prod_{j=1}^n \left(\int_{\tau_0}^{\tau_0 + \tau'} \sqrt{g_j[\theta^j(\xi)]} \frac{d\theta^j}{d\xi} d\xi \right) \right] d\tau' \right\}. \end{aligned} \quad (8)$$

We emphasize that for correlated microvariables $\{x\}$, $g(\theta)$ is not factorizable and the general definition of the IGE must be employed. For a discussion on the effects of microscopic correlations on the IGE of Gaussian statistical models, we refer to Ref. [24]. Within the IGAC, the leading asymptotic behavior of $\mathcal{S}_{\mathcal{M}_s}(\tau)$ in Eq. (8) is used to characterize the complexity of the statistical models being investigated. For this purpose, we take into consideration the leading asymptotic term in the IGE expression,

$$\mathcal{S}_{\mathcal{M}_s}^{\text{asymptotic}}(\tau) \sim \lim_{\tau \rightarrow \infty} [\mathcal{S}_{\mathcal{M}_s}(\tau)]. \quad (9)$$

We point out that $\mathcal{D}_\theta(\tau')$ specifies the integration space that appears in the definition of $\text{vol}[\mathcal{D}_\theta(\tau')]$ in Eq. (5). It is given by

$$\mathcal{D}_\theta(\tau') \stackrel{\text{def}}{=} \{\theta : \theta^j(\tau_0) \leq \theta^j \leq \theta^j(\tau_0 + \tau')\}, \quad (10)$$

where $\theta^j = \theta^j(\xi)$ with $\tau_0 \leq \xi \leq \tau_0 + \tau'$ and τ_0 denoting the initial value of the affine parameter ξ such that

$$\frac{d^2 \theta^j(\xi)}{d\xi^2} + \Gamma_{ik}^j \frac{d\theta^i}{d\xi} \frac{d\theta^k}{d\xi} = 0. \quad (11)$$

The quantities Γ_{ik}^j in Eq. (11) are the Christoffel connection coefficients,

$$\Gamma_{ik}^j \stackrel{\text{def}}{=} \frac{1}{2} g^{jl} (\partial_i g_{jk} + \partial_k g_{il} - \partial_l g_{ik}). \quad (12)$$

The integration domain $\mathcal{D}_\theta(\tau')$ is an n -dimensional subspace of $\mathcal{D}_\theta^{\text{tot}}$ whose elements are n -dimensional macrovariables $\{\theta\}$ with components θ^j bounded by given limits of integration $\theta^j(\tau_0)$ and $\theta^j(\tau_0 + \tau')$. The integration of the n -coupled nonlinear second-order ODEs in Eq. (11) determines the temporal functional form of such limits. Having defined the IGE, we call the information geometric complexity (IGC) the quantity $\mathcal{C}_{\mathcal{M}_s}(\tau)$ defined as

$$\mathcal{C}_{\mathcal{M}_s}(\tau) \stackrel{\text{def}}{=} \widetilde{\text{vol}}[\mathcal{D}_\theta(\tau)] = e^{\mathcal{S}_{\mathcal{M}_s}(\tau)}. \quad (13)$$

In particular, we shall focus on the asymptotic temporal behavior of the complexity as described by $\mathcal{C}_{\mathcal{M}_s}^{\text{asymptotic}}(\tau) \stackrel{\tau \rightarrow \infty}{\sim} e^{\mathcal{S}_{\mathcal{M}_s}(\tau)}$.

To interpret $\mathcal{C}_{\mathcal{M}_s}(\tau)$, we simply give an interpretation of $\mathcal{S}_{\mathcal{M}_s}(\tau)$. This latter quantity is defined in Eq. (3) as an affine temporal average of the n -fold integral of the Fisher density over geodesic paths viewed as maximum probability trajectories and serves as a measure of the number of the accessible macrostates in the statistical configuration manifold. More specifically, the IGE at a specific instant is defined as the logarithm of the volume of the effective parameter space explored by the system at that very instant. We introduce the temporal averaging procedure in Eq. (4) to average out the possibly very complex fine details of the entropic dynamical description of the system on the underlying curved statistical manifold. Furthermore, we consider the long-time limit in Eq. (9) to characterize in a proper fashion the chosen dynamical indicators of chaoticity by removing the transient effects which enter the computation of the expected value of the volume of the effective parameter space. Therefore, the IGE is constructed to provide an asymptotic coarse-grained inferential description of the complex dynamics of a system in the presence of incomplete information. For further details on the IGE and IGC, we refer to Refs. [25–27].

In this paper, we focus on quantifying the IGC of parametrized probability paths $\{p_x(\theta)\}$ with $p_x(\theta) \stackrel{\text{def}}{=} p(x|\theta)$ constructed from the time-dependent transition probabilities between orthogonal initial and final quantum states $\{|w\rangle, |w_\perp\rangle\}$ emerging from selected quantum mechanical evolutions of two-level quantum systems (see Sec. IV). The single parameter θ used in the parametrization can be regarded as the statistical version of the elapsed time t . In particular, θ is assumed to be an experimental parameter that can be characterized by measuring a suitable time-dependent observable quantity such as the transverse magnetic field intensity $B_\perp(t)$.

Having introduced the IGC concept in Eq. (13), we propose our measure of entropic efficiency in the next section.

III. EFFICIENCY

In this section, after recalling the notions of thermodynamic length and thermodynamic divergence, we propose our measure of entropic efficiency.

A. Thermodynamic length and divergence

Thermodynamic systems can be specified by Riemannian manifolds equipped with a thermodynamic metric tensor that is identical to the Fisher information metric [28], once the theory of fluctuations is included into the axioms of equilibrium thermodynamics [29]. Then, this Riemannian structure allows one to define the notion of length for fluctuations about equilibrium states as well as for thermodynamic processes proceeding via equilibrium states. Originally, Weinhold presented a Riemannian metric in the space of thermodynamic equilibrium states employing the second derivatives of the internal energy with respect to extensive variables in Ref. [30]. Subsequently, Ruppeiner proposed a Riemannian geometric model of thermodynamics with a Riemann structure defined by means of a metric tensor specified by second derivatives of the entropy as a function of extensive variables (such as volume and mole number, for instance) in Ref. [29]. Salamon and Berry introduced the notion of thermodynamic length by employing the energy version of the thermodynamic metric tensor $g_{\alpha\beta}(\theta)$ in Ref. [31],

$$\mathcal{L}(\bar{\tau}/\tau_*) \stackrel{\text{def}}{=} \int_0^{\bar{\tau}/\tau_*} \left(\frac{d\theta^\alpha}{dt_{\text{th}}} g_{\alpha\beta}(\theta) \frac{d\theta^\beta}{dt_{\text{th}}} \right)^{1/2} dt_{\text{th}}, \quad (14)$$

with t_{th} denoting the dimensionless thermodynamic time t_{th} with $0 \leq t_{\text{th}} \leq \bar{\tau}/\tau_*$. Furthermore, $\bar{\tau}$ and τ_* are the duration time and the mean internal relaxation time of the physical process under consideration, respectively. For clarity, we point out that the mean relaxation time τ_* is an indicator of how fast the physical system reaches an equilibrium configuration with an environment with which it is brought into contact. In particular, to a smaller value of τ_* there corresponds a faster equilibration of the system-environment system. For a detailed discussion on the concepts of instantaneous and mean relaxation times in molecular physics, we refer to Ref. [32]. Upon identifying the affine parameter ξ with the dimensionless thermodynamic time t_{th} and the duration of the process τ with $\bar{\tau}/\tau_*$, the thermodynamic length in Eq. (14) of a path γ_θ with the parameter θ parametrized by an affine parameter ξ with $0 \leq \xi \leq \tau$ in the space of thermal states becomes

$$\mathcal{L}(\tau) = \int_0^\tau \left(\frac{d\theta^\alpha}{d\xi} g_{\alpha\beta}(\theta) \frac{d\theta^\beta}{d\xi} \right)^{1/2} d\xi. \quad (15)$$

The quantity $\mathcal{L}(\tau)$ in Eq. (15) is measured by the number of natural fluctuations along the path γ_θ . The larger the fluctuations, the closer the points are together. Indeed, in analogy to Wootters' statistical distance between probability distributions [33], the thermodynamic length can be interpreted as a measure of the maximal number of statistically distinguishable thermodynamic states along the path γ_θ [34]. As a matter of fact, following Wootters, we can interpret the points θ and $\theta + d\theta$ long the path γ_θ as statistically distinguishable if $d\theta$ is at least equal to the standard fluctuation of θ . In terms of the distance $ds^2 = g_{\alpha\beta}(\theta)d\theta^\alpha d\theta^\beta$, this is equivalent to

$ds^2 \geq 1$. Clearly, $\mathcal{L}(\tau)$ in Eq. (15) has dimensions of (energy)^{1/2} if one uses the energy version of the thermodynamic metric tensor. If, instead, one uses the entropy version of the thermodynamic metric tensor, then $\mathcal{L}(\tau)$ has dimensions of (entropy)^{1/2}. To better understand the physical interpretation of the thermodynamic length, it is helpful to introduce the so-called thermodynamic divergence $\mathcal{I}(\tau)$ of a path γ_θ with the variable θ expressed in terms of an affine parameter ξ with $0 \leq \xi \leq \tau$ as in Eq. (15),

$$\mathcal{I}(\tau) \stackrel{\text{def}}{=} \int_0^\tau \frac{d\theta^\alpha}{d\xi} g_{\alpha\beta}(\theta) \frac{d\theta^\beta}{d\xi} d\xi. \quad (16)$$

The quantity $\mathcal{I}(\tau)$ in Eq. (16) is a measure of the losses (or, dissipation) in the process quantified by the total entropy produced (or dissipated availability [31]) along the path γ_θ . Applying the Cauchy-Schwarz inequality with integrals of functions,

$$\left[\int_0^\tau f_1^2(\xi) d\xi \right] \left[\int_0^\tau f_2^2(\xi) d\xi \right] \geq \left[\int_0^\tau f_1(\xi) f_2(\xi) d\xi \right]^2, \quad (17)$$

and using Eqs. (15) and (16), it happens that $\mathcal{I} \geq \tau^{-1} \mathcal{L}^2$ with $\tau \stackrel{\text{def}}{=} \bar{\tau}/\tau_*$ once we identify $f_1(\xi)$ and $f_2(\xi)$ with $ds/d\xi$ and 1, respectively. Therefore, the square of the thermodynamic length of the path γ_θ multiplied by the ratio of the internal relaxation time of the system to the duration of the process furnishes a lower bound to the dissipation in the process. This bound is more realistic than the (ideal) reversible bound which would be equal to zero. The equality $\mathcal{I} = \mathcal{I}_{\text{min}} \stackrel{\text{def}}{=} \tau^{-1} \mathcal{L}^2$ is obtained when the thermodynamic speed is constant along the path γ_θ . Therefore, the process exhibits minimum losses when it produces minimum entropy. This happens when it proceeds at constant speed, with the entropy production rate being equal to the squared thermodynamic speed itself.

Let $n_{\mathcal{M}_\xi}$ be the dimensionality of the parameter space with $\theta(\xi) \stackrel{\text{def}}{=} \{\theta^\alpha(\xi)\}_{1 \leq \alpha \leq n_{\mathcal{M}_\xi}}$ and $0 \leq \xi \leq \tau$. Then, the optimum paths γ_θ are paths characterized by the most favorable affine time ξ parametrization yielding the shortest thermodynamic length. More explicitly, the optimum paths satisfy the geodesic equation that can be obtained via variational calculus by minimizing the action functional represented by the thermodynamic length in Eq. (15). One imposes that $\delta \mathcal{L}$ is equal to zero subject to the constraint that $\delta \theta^\alpha = 0$ at the extremum. We point out that ξ is defined up to changes of scale and origin and, thus, is not unique. Interestingly, we emphasize that the optimum paths that minimize $\mathcal{L}(\tau)$ in Eq. (15) are the paths that minimize the divergence $\mathcal{I}(\tau)$ in Eq. (16). As a matter of fact, minimizing $\mathcal{I}(\tau)$ under the same working conditions used in the minimization of $\mathcal{L}(\tau)$, it happens that the optimum paths $\theta^\alpha(\xi)$ satisfy the equation

$$\frac{d}{d\xi} \left[g_{\alpha\rho}(\theta) \frac{d\theta^\alpha}{d\xi} \right] - \frac{1}{2} \frac{d\theta^\alpha}{d\xi} \frac{\partial g_{\alpha\beta}(\theta)}{\partial \theta^\rho} \frac{d\theta^\beta}{d\xi} = 0. \quad (18)$$

It is worth noting that Eq. (18) is the information geometric analogue of Eqs. (36) and (6) in Refs. [35,36], respectively. For an explicit verification of the interchangeability between the geodesic equations emerging from the variations of $\delta(\int \sqrt{ds^2})$ and $\delta(\int ds^2)$, we refer to Appendix A. Since optimum paths are geodesic paths, the ‘‘thermodynamic’’ speed

is constant when evaluated along these shortest paths. Henceforth, we shall name this speed “entropic” speed v_E and define it as

$$v_E \stackrel{\text{def}}{=} \left[\frac{d\theta^\alpha}{d\xi} g_{\alpha\beta}(\theta) \frac{d\theta^\beta}{d\xi} \right]^{1/2}. \quad (19)$$

Moreover, optimum paths are also paths specified by constant entropy production rate r_E (that is, the squared invariant norm of the speed v_E), with r_E given by

$$r_E \stackrel{\text{def}}{=} \frac{d}{d\tau} \mathcal{I}(\tau) = \frac{d}{d\tau} \left[\int_0^\tau \frac{d\theta^\alpha}{d\xi} g_{\alpha\beta}(\theta) \frac{d\theta^\beta}{d\xi} d\xi \right], \quad (20)$$

with the thermodynamic divergence $\mathcal{I}(\tau)$ defined in Eq. (16) and evaluated along the optimum paths. For clarity, we stress that we are interested here in the global (i.e., integral) problem of minimizing the entropy production over the complete path. Alternatively, one may be interested in the local (i.e., differential) problem of minimizing the rate of entropy dissipation at each instant of time [37]. Moreover, for completeness, we point out that both minimum entropy production and constant entropy production rate occur along geodesic paths in thermodynamic state space for optimal (linear) processes with $g_{\alpha\beta} = g_{\alpha\beta}(\theta)$. For a discussion on the nonconstancy of the rate of entropy production within the framework of nonlinearized thermodynamics of irreversible processes with $g_{\alpha\beta} = g_{\alpha\beta}(\theta, \dot{\theta})$, we refer to Ref. [38].

To better grasp the physical interpretation of r_E in Eq. (20), we note two facts. First, the thermodynamic metric tensor $g_{\alpha\beta}(\theta)$ equals $\overline{\delta X_{\alpha\beta}^2}$, with

$$\overline{\delta X_{\alpha\beta}^2} \stackrel{\text{def}}{=} \langle (X_\alpha - \langle X_\alpha \rangle)(X_\beta - \langle X_\beta \rangle) \rangle. \quad (21)$$

The quantity $\overline{\delta X_{\alpha\beta}^2}$ in Eq. (21) is the covariance matrix of fluctuations around equilibrium defined in terms of the thermodynamic variables $\{X_\alpha(x)\}$ that characterize the Hamiltonian of the system. The quantity $\{x\}$ denotes the set of relevant configuration space variables. Second, consider the canonical Gibbs distribution function $p(x|\theta) \equiv p_x(\theta)$ with $p_x(\theta)$ defined as

$$p_x(\theta) \stackrel{\text{def}}{=} \frac{e^{-\theta^\alpha(\xi)X_\alpha(x)}}{\mathcal{Z}}, \quad (22)$$

with \mathcal{Z} being the partition function of the system. Inserting $p_x(\theta)$ in Eq. (22) into the usual definition of the Fisher-Rao information metric tensor $g_{\alpha\beta}(\theta)$, it can be shown that this latter quantity equals the thermodynamic metric tensor. In other words, $g_{\alpha\beta}(\theta)$ is equal to $\overline{\delta X_{\alpha\beta}^2}$ in Eq. (21). Then, a simple calculation yields the following alternative expression of r_E in Eq. (20),

$$r_E = \frac{d\theta^\alpha}{d\xi} \overline{\delta X_{\alpha\beta}^2} \frac{d\theta^\beta}{d\xi} = \sum_x p_x(\theta) \left(\frac{d \log p_x(\theta)}{d\xi} \right)^2, \quad (23)$$

Therefore, r_E in Eq. (23) can be also described as the “product” of the fluctuation term $\overline{\delta X_{\alpha\beta}^2}$ and the square of the total rate of change with respect to the affine parameter ξ of the control parameter $\theta^\alpha(\xi)$. Note that in heat transfer problems, be it cooling or heating, the control parameter is given by temperature. However, in mass transfer problems, in magnetic

systems, and in elastic systems, suitable control parameters are specified by chemical potential, magnetic field, and stress, respectively. For a more detailed discussion on the physical significance of the concept of entropy production rate in relation to the thermodynamics of a system of spin-1/2 particles driven by an external magnetic field, we refer to Appendix B. For the sake of forthcoming discussions, we shall be naming lengths, divergences, and speeds as “entropic” quantities.

B. Entropic efficiency

In what follows, we propose an efficiency measure η_E with $0 \leq \eta_E \leq 1$ for the various driving schemes in terms of the rate of entropy production r_E along the path γ_θ .

In Ref. [14], we proposed an asymmetric efficiency measure $\eta_E^{(1)}$ where the hottest path corresponded to the least efficient driving scheme. The efficiency $\eta_E^{(1)}$ was defined as

$$\eta_E^{(1)}(r_E) \stackrel{\text{def}}{=} 1 - \frac{r_E}{r_E^{\max}}, \quad (24)$$

where $0 \leq \eta_E^{(1)}(r_E) \leq 1$ for any $0 \leq r_E \leq r_E^{\max}$ with $\eta_E^{(1)}(r_E^{\max}) = 0$. This efficiency was partially inspired by the definition of thermal efficiency of a heat engine [39] and by the notion of efficiency of a quantum evolution in the Riemannian approach to quantum mechanics as presented in Refs. [40,41]. The thermal efficiency η_{thermo} of a heat engine in thermodynamics can be defined as

$$\eta_{\text{thermo}} \stackrel{\text{def}}{=} 1 - \frac{Q_{\text{out}}}{Q_{\text{in}}}, \quad (25)$$

with Q_{out} and Q_{in} being the output and input thermal energies with $W_{\text{out}} \stackrel{\text{def}}{=} Q_{\text{in}} - Q_{\text{out}} \geq 0$ denoting the actual work performed by the heat engine [39]. In the Riemannian approach to quantum mechanics, instead, the efficiency of a quantum evolution is defined as $\eta_{\text{QM}} \stackrel{\text{def}}{=} 1 - \Delta s/s$ with $0 \leq \eta_{\text{QM}} \leq 1$ and $\Delta s \stackrel{\text{def}}{=} s - s_0$. The quantity s_0 represents the dimensionless distance along the shortest geodesic path (ideal) γ_{ideal} joining the fixed initial ($|A\rangle$) and final ($|B\rangle$) points of the evolution that are distinct points on the complex projective Hilbert space. The quantity s instead, denotes the distance along the effective (real) path γ_{real} connecting $|A\rangle$ and $|B\rangle$ and is measured by the Fubini-Study metric. The quantum evolution is maximally efficient when the evolution occurs with minimum time-energy uncertainty. This scenario is specified by $\eta_{\text{QM}} = 1$ and happens when γ_{real} and s approach γ_{ideal} and s_0 , respectively. Concerning this latter inspiration, we replaced the quantum mechanical condition of maximum energy dispersion with the information-theoretic requirement of minimum entropy production. Then, we found it appropriate to propose a definition of entropic efficiency of an evolution along a path of minimum entropic length joining the distinct initial and final points on the information manifold as the above mentioned quantity $\eta_E^{(1)}(r_E)$. In this efficiency definition, r_E^{\max} plays the effective role of a normalizing factor that makes η_E adimensional with $0 \leq \eta_E^{(1)}(r_E) \leq 1$. Then, unit entropic efficiency can be achieved when the evolution is characterized by a path that is maximally cooled (that is, maximally reversible). In such a case, the total entropy production remains ideally constant

during the evolution and, as a consequence, the rate of entropy production r_E vanishes. Alternatively, one may think of proposing a different asymmetric efficiency measure $\eta_E^{(2)}(r_E)$ where the coolest path is the most efficient. In this case, one can propose a measure $\eta_E^{(2)}(r_E)$ given by

$$\eta_E^{(2)}(r_E) \stackrel{\text{def}}{=} \frac{r_E^{\min}}{r_E}, \quad (26)$$

where $0 \leq \eta_E^{(2)}(r_E) \leq 1$ for any $0 \leq r_E^{\min} \leq r_E$ with $\eta_E^{(2)}(r_E^{\min}) = 1$. We point out that both measures $\eta_E^{(1)}(r_E)$ in Eq. (24) and $\eta_E^{(2)}(r_E)$ in Eq. (26) preserve the relative ranking of paths. In addition, they are asymmetric measures since r_E^{\max} and r_E^{\min} play special roles in the ranking procedure. However, in both ranking schemes, r_E^{\max} and r_E^{\min} belong to the set of entropy production rates that specify the paths being ranked. Specifically, $r_E^{\min} = r_E^{(k)}$ and $r_E^{\max} = r_E^{(k')}$ belong to $\{r_E^{(i)}\}_{1 \leq i \leq \bar{N}}$ for some $k \neq k' \in \{1, \dots, \bar{N}\}$ with \bar{N} denoting the number of driving schemes being ranked. Therefore, r_E^{\min} (r_E^{\max}) does not represent an absolute external minimum (maximum) to be achieved in an ideal best (worst) scenario. Moreover, depending on the particular tuning of the parameters that specify the driving Hamiltonian, r_E^{\min} and r_E^{\max} can change. More explicitly, assuming the tuning of a single parameter (for instance, the frequency of oscillation of a time-dependent external magnetic field), there could be a range of values of this parameter for which $(r_E^{\min}, r_E^{\max}) = (r_E^{(k)}, r_E^{(k')})$ and a different range for which $(r_E^{\min}, r_E^{\max}) = (r_E^{(\tilde{k})}, r_E^{(\tilde{k}')})$ with $k \neq \tilde{k}$ and/or $k' \neq \tilde{k}'$. Motivated by the lack of an absolute optimal driving scheme of reference (unlike the quantum scenarios studied in Refs. [40,41]) and maintaining the willingness of preserving the idea of dependence of the entropic efficiency on the rate of entropy production (with the coolest paths being the most efficient and the hottest paths being the least efficient), we propose in this paper a symmetric measure of entropic efficiency given by

$$\eta_E(r_E^{(l)}, r_E^{(m)}) \stackrel{\text{def}}{=} 1 - \frac{|r_E^{(l)} - r_E^{(m)}|}{r_E^{(l)} + r_E^{(m)}}, \quad (27)$$

with $0 \leq \eta_E(r_E^{(l)}, r_E^{(m)}) \leq 1$ by construction for any pair of positive $r_E^{(l)}$ and $r_E^{(m)}$. Furthermore, $\eta_E(r_E^{(l)}, r_E^{(m)})$ preserves the relative ranking of paths that one obtains by means of $\eta_E^{(1)}(r_E)$ and $\eta_E^{(2)}(r_E)$. For an explicit check of this conservation behavior, we refer to Appendix C. Clearly, although preserving the relative ranking of paths, $\eta_E^{(1)}(r_E)$ and $\eta_E^{(2)}(r_E)$ assume relatively different numerical values. For instance, while $\eta_E^{(2)}(r_E) \rightarrow 1$ as $r_E \rightarrow r_E^{\min}$, $\eta_E^{(1)}(r_E) \rightarrow 1$ in the extreme scenario in which $r_E \rightarrow 0$. Moreover, while $\eta_E^{(1)}(r_E) \rightarrow 0$ as $r_E \rightarrow r_E^{\max}$, $\eta_E^{(2)}(r_E) \rightarrow 0$ in the extreme scenario in which $r_E \rightarrow \infty$. In our paper, one of the two values between $r_E^{(l)}$ and $r_E^{(m)}$ (say, $r_E^{(m)}$) is picked as r_E^{\min} for a given range of values of the Hamiltonian parameter being tuned. Then, our proposed measure of efficiency assumes unit value when $r_E^{(l)} = r_E^{(m)}$ with $r_E^{(m)} \stackrel{\text{def}}{=} r_E^{\min}$ and tends to vanish when $r_E^{(l)} \gg r_E^{\min}$. For a detailed physical discussion on the idea of irreversible entropy production when analyzing the causes of inefficiency in thermodynamic systems, we refer to Ref. [42].

Having introduced the IGC in Eq. (13) and the entropic efficiency in Eq. (27), we are ready to describe the quantum driving schemes that we study in the next section.

IV. QUANTUM DRIVING SCHEMES

In this section, we introduce the quantum driving schemes being investigated and mention the manner in which one can generate probability paths from the output quantum pure state emerging from the quantum mechanical evolution.

A. Probability paths from driving schemes

Inspired by the link between analog quantum search and two-level quantum systems [16,43] and following Refs. [14,44], we suppose that the normalized output quantum state of a $\text{su}(2; \mathbb{C})$ time-dependent Hamiltonian mimicking a continuous-time quantum search algorithm can be described as

$$|\psi(\theta)\rangle \stackrel{\text{def}}{=} e^{i\varphi_w(\theta)} \sqrt{p_w(\theta)} |w\rangle + e^{i\varphi_{w_\perp}(\theta)} \sqrt{p_{w_\perp}(\theta)} |w_\perp\rangle, \quad (28)$$

where the input is the normalized $N \stackrel{\text{def}}{=} 2^n$ -dimensional n -qubit source state $|s\rangle \stackrel{\text{def}}{=} |\psi(\theta_0)\rangle$. Observe that $|\psi(\theta)\rangle$ belongs to the two-dimensional subspace of \mathcal{H}_2^n , the n -qubit complex Hilbert space spanned by the set of orthonormal state vectors $\{|w\rangle, |w_\perp\rangle\}$ and containing $|s\rangle$. Furthermore, $\varphi_w(\theta)$ and $\varphi_{w_\perp}(\theta)$ denote real quantum phases of the states $|w\rangle$ and $|w_\perp\rangle$, respectively. Taking our source state $|s\rangle$ to be identified with $|w_\perp\rangle$, our analysis will focus on the space of probability distributions $\{p(\theta)\}$ with $p(\theta) \stackrel{\text{def}}{=} (p_w(\theta), p_{w_\perp}(\theta))$ where $p_w(\theta) \stackrel{\text{def}}{=} |\langle w|\psi(\theta)\rangle|^2$ and $p_{w_\perp}(\theta) \stackrel{\text{def}}{=} |\langle w_\perp|\psi(\theta)\rangle|^2$ specify the success and failure probabilities of the driving Hamiltonian, respectively. For clarity, we underline that $\mathcal{X} \stackrel{\text{def}}{=} \{x\} = \{w, w_\perp\}$ forms here the space of configuration variables with $p_x(\theta)$ being a probability mass function since $\{x\}$ is a discrete set. In particular, the space of probability distributions $\{p(\theta)\}$ is equipped with the natural Riemannian distinguishability metric given by the Fisher information metric $g_{\alpha\beta}(\theta)$. In the case of a discrete microspace \mathcal{X} , $g_{\alpha\beta}(\theta)$ is defined as

$$g_{\alpha\beta}(\theta) \stackrel{\text{def}}{=} \sum_{x \in \mathcal{X}} p_x(\theta) \partial_\alpha \log [p_x(\theta)] \partial_\beta \log [p_x(\theta)]. \quad (29)$$

Furthermore, under suitably chosen working conditions [45], $g_{\alpha\beta}(\theta)$ can be taken to be proportional to the Fubini-Study metric. Indeed, the Fubini-Study metric can be written as $g_{\alpha\beta}^{\text{FS}}(\theta) = (1/4)[g_{\alpha\beta}(\theta) + 4\sigma_{\alpha\beta}^2(\theta)] \propto g_{\alpha\beta}(\theta)$ when the variance of the phase changes $\sigma_{\alpha\beta}^2(\theta)$ is equal to zero. It happens that one can always set this term equal to zero provided that one rephases in a favorable manner the basis vectors used in the decomposition of $|\psi(\theta)\rangle$ as originally discussed in Ref. [45]. We emphasize that the output state $|\psi(\theta)\rangle$ is parametrized in terms of a single continuous real parameter θ that emerges from the elapsed computing time t of the algorithm (or, equivalently, driving Hamiltonian). The parameter θ , a statistical version of t , plays the role of a statistical macrovariable employed to distinguish neighboring quantum states $|\psi(\theta)\rangle$ and $|\psi(\theta)\rangle + |d\psi(\theta)\rangle$ along a path through the space of quantum mechanical pure states. It can be viewed

as an experimental parameter that can be determined by measurement of a conventional observable that varies with time such as a time-dependent transverse magnetic field intensity. Our main objective here is to calculate the IGC of the optimum cooling paths, that is paths on the manifold of state space parametrized by θ along which one drives the system while minimizing the entropy production. Then, after evaluating the entropic efficiency of each driving scheme being considered, we wish to find out whether or not there is any link between this entropic efficiency and the IGC of the optimum cooling paths generated by the driving schemes themselves.

In what follows, we describe how the normalized pure states $\{|\psi(\theta)\rangle\}$ that we consider emerge as outputs of suitable $\text{su}(2; \mathbb{C})$ time-dependent Hamiltonian evolutions that mimic quantum search Hamiltonian motion.

B. Quantum driving schemes

We recall that $\text{su}(2; \mathbb{C})$ is the Lie algebra of the special unitary group $\text{SU}(2; \mathbb{C})$ and is generated by three traceless and anti-Hermitian generators $\{i\sigma_x, -i\sigma_y, i\sigma_z\}$ where $\vec{\sigma} \stackrel{\text{def}}{=} (\sigma_x, \sigma_y, \sigma_z)$ is the Pauli vector operator [46]. We study quantum evolutions specified by means of Hamiltonian operators $\mathcal{H}_{\text{su}(2; \mathbb{C})}(t)$ defined as

$$\mathcal{H}_{\text{su}(2; \mathbb{C})}(t) \stackrel{\text{def}}{=} a(t)(i\sigma_x) + b(t)(-i\sigma_y) + c(t)(i\sigma_z), \quad (30)$$

with $a(t)$, $b(t)$, and $c(t)$ being time-dependent complex coefficients. Adopting the $\text{su}(2; \mathbb{C})$ -Hamiltonian models terminology, let us introduce the concepts of complex transverse field and real longitudinal field, denoted as $\omega(t) \stackrel{\text{def}}{=} \omega_x(t) - i\omega_y(t) = \omega_{\mathcal{H}}(t)e^{i\phi_{\omega}(t)}$ and $\Omega(t)$, respectively. Obviously, $\omega_{\mathcal{H}}(t)$ represents the modulus $|\omega(t)|$ of $\omega(t)$. Then, setting $a(t) \stackrel{\text{def}}{=} -i\omega_x(t)$, $b(t) \stackrel{\text{def}}{=} i\omega_y(t)$, and $c(t) \stackrel{\text{def}}{=} -i\Omega(t)$, the $\text{su}(2; \mathbb{C})$ -Hamiltonian becomes

$$\mathcal{H}_{\text{su}(2; \mathbb{C})}(t) \stackrel{\text{def}}{=} \omega_x(t)\sigma_x + \omega_y(t)\sigma_y + \Omega(t)\sigma_z. \quad (31)$$

We assume that the transverse fields $\omega(t)$ lie in the xy -plane while the longitudinal fields $\Omega(t)$ are oriented along the z -axis. We observe that the $\text{su}(2; \mathbb{C})$ -Hamiltonian can be recast as $\mathcal{H}_{\text{su}(2; \mathbb{C})}(t) \stackrel{\text{def}}{=} -\vec{\mu} \cdot \vec{B}(t)$ when taking into consideration the evolution of a spin-1/2 particle in an external time-dependent magnetic field $\vec{B}(t)$. As usual, $\vec{\mu} \stackrel{\text{def}}{=} (e\hbar/2mc)\vec{\sigma}$ denotes the magnetic moment of the electron with $\mu_{\text{Bohr}} \stackrel{\text{def}}{=} e\hbar/(2mc)$ being the so-called Bohr magneton. The quantity $|e|$ denotes the absolute value of the electric charge of an electron while m is the mass of an electron. Moreover, \hbar and c denote the reduced Planck constant and the speed of light, respectively. To understand the relation between the set of field intensities $\{\omega_{\mathcal{H}}(t), \Omega_{\mathcal{H}}(t)\}$ and the magnetic field $\vec{B}(t)$, we decompose $\vec{B}(t)$ as $\vec{B}(t) \stackrel{\text{def}}{=} \vec{B}_{\perp}(t) + \vec{B}_{\parallel}(t)$, with $\vec{B}_{\perp}(t) \stackrel{\text{def}}{=} B_x(t)\hat{x} + B_y(t)\hat{y}$ and $\vec{B}_{\parallel}(t) \stackrel{\text{def}}{=} B_z(t)\hat{z}$. Then, it follows that $B_{\perp}(t) \propto \omega_{\mathcal{H}}(t) \stackrel{\text{def}}{=} |\omega(t)|$ and $B_{\parallel}(t) \propto \Omega_{\mathcal{H}}(t) \stackrel{\text{def}}{=} |\Omega(t)|$. More specifically, the exact relation in terms of field components between $\{B_x(t), B_y(t), B_z(t)\}$ and $\{\omega_x(t), \omega_y(t), \Omega(t)\}$ is

expressed by the equalities

$$\begin{aligned} B_x(t) &= -\frac{2mc}{e\hbar}\omega_x(t), B_y(t) = -\frac{2mc}{e\hbar}\omega_y(t), \text{ and} \\ B_z(t) &= -\frac{2mc}{e\hbar}\Omega(t). \end{aligned} \quad (32)$$

Furthermore, in terms of field intensities $B_{\perp}(t)$ and $B_{\parallel}(t)$, one obtains

$$B_{\perp}(t) = \frac{2mc}{|e|\hbar}\omega_{\mathcal{H}}(t), \text{ and } B_{\parallel}(t) = \frac{2mc}{|e|\hbar}\Omega_{\mathcal{H}}(t). \quad (33)$$

Despite its apparent simplicity, it is a highly challenging matter studying the evolution of an electron specified by the Hamiltonian $\mathcal{H}_{\text{su}(2; \mathbb{C})}(t)$ by means of exact analytical expressions of complex probability amplitudes and real transition probabilities from an initial source state to a final target state. The quantum mechanical time propagator $\mathcal{U}(t)$,

$$\mathcal{U}(t) \stackrel{\text{def}}{=} \begin{pmatrix} \alpha(t) & \beta(t) \\ -\beta^*(t) & \alpha^*(t) \end{pmatrix}, \quad (34)$$

with $i\hbar\dot{\mathcal{U}}(t) = \mathcal{H}_{\text{su}(2; \mathbb{C})}\mathcal{U}(t)$ and $\dot{\mathcal{U}} \stackrel{\text{def}}{=} \partial_t\mathcal{U}$, is unitary and demands that the probability amplitudes $\alpha(t)$ and $\beta(t)$ must satisfy the normalization condition $|\alpha(t)|^2 + |\beta(t)|^2 = 1$. Then, $\{|w\rangle, |w_{\perp}\rangle\}$ being a set of orthonormal state vectors that span the two-dimensional search space of the \mathcal{H}_2^2 , the time evolution of a source state $|s\rangle \stackrel{\text{def}}{=} x|w\rangle + \sqrt{1-x^2}|w_{\perp}\rangle$ with $x \stackrel{\text{def}}{=} \langle w|s\rangle$ can be described by the mapping,

$$\begin{aligned} (x, \sqrt{1-x^2}) &\xrightarrow{\mathcal{U}(t)} (\alpha(t)x + \beta(t)\sqrt{1-x^2}, -\beta^*(t)x \\ &+ \alpha^*(t)\sqrt{1-x^2}). \end{aligned} \quad (35)$$

Thus, the probability $\mathcal{P}_{|s\rangle \rightarrow |w\rangle}(t)$ that under $\mathcal{U}(t)$ the source state $|s\rangle$ transitions into the target state $|w\rangle$ becomes

$$\begin{aligned} \mathcal{P}_{|s\rangle \rightarrow |w\rangle}(t) &\stackrel{\text{def}}{=} |\langle w|\mathcal{U}(t)|s\rangle|^2 \\ &= |\alpha(t)|^2x^2 + |\beta(t)|^2(1-x^2) \\ &+ [\alpha(t)\beta^*(t) + \alpha^*(t)\beta(t)]x\sqrt{1-x^2}. \end{aligned} \quad (36)$$

As evident from Eq. (36), it is necessary to possess the exact analytical expression of the evolution operator $\mathcal{U}(t)$ in terms of the complex probability amplitudes $\alpha(t)$ and $\beta(t)$ to calculate the exact analytical expression of $\mathcal{P}_{|s\rangle \rightarrow |w\rangle}(t)$. For completeness, a general parametrization of $\alpha(t)$ and $\beta(t)$ is given in Appendix D. Inspired by our results reported in Ref. [16] and, above all, making use of the findings in Refs. [17, 18], we focus our attention on four distinct quantum mechanical driving scenarios where $\mathcal{P}_{|w_{\perp}\rangle \rightarrow |w\rangle}(t)$ can be analytically expressed. The states $|w\rangle$ and $|w_{\perp}\rangle$ with $\langle w_{\perp}|w\rangle = \delta_{w_{\perp}, w}$ are chosen so that $\sigma_z|w\rangle = +|w\rangle$ and $\sigma_z|w_{\perp}\rangle = -|w_{\perp}\rangle$. The quantity that specifies the four scenarios is the modulus $|\omega(t)|$ of the complex transverse field $\omega(t)$, $\omega_{\mathcal{H}}(t) \stackrel{\text{def}}{=} |\omega(t)| \propto B_{\perp}(t)$. However, for experimental convenience, we assume that $\phi_{\omega}(t) = \omega_0$ and $\Omega(t) = -(\hbar/2)\omega_0$ with ω_0 a negative constant in all four scenarios. More general temporal behaviors $\phi_{\omega}(t)$ and $\Omega(t)$ can be chosen provided that the so-called generalized Rabi condition $\dot{\phi}_{\omega}(t) + (2/\hbar)\Omega(t) = 0$ is satisfied as pointed out in Ref. [17, 18]. The first case specifies the original Rabi scenario where we assume a constant field intensity

$\omega_{\mathcal{H}}^{(1)}(t) \stackrel{\text{def}}{=} \Gamma$ with $\mathcal{P}_{|w_{\perp}\rangle \rightarrow |w\rangle}^{(1)}(t) = \sin^2[(\Gamma/\hbar)t]$. The remaining three cases are generalized Rabi scenarios with field intensity assumed to be exhibiting oscillatory, power law decay, and exponential law decay behaviors. In summary, we have

$$\begin{aligned} \omega_{\mathcal{H}}^{(1)}(t) &\stackrel{\text{def}}{=} \Gamma, \omega_{\mathcal{H}}^{(2)}(t) \stackrel{\text{def}}{=} \Gamma \cos(\lambda t), \omega_{\mathcal{H}}^{(3)}(t) \\ &\stackrel{\text{def}}{=} \Gamma/(1 + \lambda t)^2, \text{ and } \omega_{\mathcal{H}}^{(4)}(t) \stackrel{\text{def}}{=} \Gamma e^{-\lambda t}. \end{aligned} \quad (37)$$

Note that $\omega_{\mathcal{H}}^{(2)}(t) \geq 0$ for $0 \leq t \leq (\pi/2)\lambda^{-1}$. In all four cases, it happens that $\mathcal{P}_{|w_{\perp}\rangle \rightarrow |w\rangle}^{(j)}(t)$ with $1 \leq j \leq 4$ is given by [18]

$$\mathcal{P}_{|w_{\perp}\rangle \rightarrow |w\rangle}^{(j)}(t) = \sin^2 \left[\int_0^t \frac{\omega_{\mathcal{H}}^{(j)}(t')}{\hbar} dt' \right]. \quad (38)$$

Interestingly, since the resonance condition is satisfied, $\mathcal{P}_{|w_{\perp}\rangle \rightarrow |w\rangle}^{(j)}(t)$ in Eq. (38) depends only on the integral of the transverse field intensity $\omega_{\mathcal{H}}(t)$. The transition probabilities $\mathcal{P}_{|w_{\perp}\rangle \rightarrow |w\rangle}^{(k)}(t)$ in Eq. (38) are the key ingredients that we exploit to provide an expression of the parametrized output quantum states $|\psi(\theta)\rangle$.

Having introduced the IGC in Eq. (13), the entropic efficiency in Eq. (27), and our chosen quantum mechanical driving schemes, we are ready to apply our proposed theoretical analysis.

V. APPLICATIONS

In this section, we apply our theoretical construct to four distinct quantum mechanical driving scenarios.

To apply our scheme, we need to find the optimum cooling (probability) paths before evaluating the information geometric complexity $\mathcal{C}_{\mathcal{M}_s}$ in Eq. (13), the entropic speed v_E in Eq. (19), the rate of entropy production r_E in Eq. (20), and the entropic efficiency η_E in Eq. (27) along these geodesic trajectories. To find these paths $\gamma_{\theta} : \theta \mapsto p(\theta)$ with $\theta = \theta(\xi)$ and ξ being an affine parameter, we proceed as follows. For each Schrödinger evolution characterized by a specific expression of $\omega_{\mathcal{H}}(t)$ [that is, the modulus of the complex transverse field $\omega(t)$ that is proportional to $B_{\perp}(t)$], we arrive at the regular probability paths $\{p(\theta)\}$ with $p(\theta) \stackrel{\text{def}}{=} [p_w(\theta), p_{w_{\perp}}(\theta)]$ as prescribed in the previous section. Then, having $\{p(\theta)\}$, we calculate the Fisher information $g(\theta) = E_{\theta}[\{\partial_{\theta} \log[p_x(\theta)]\}^2]$ with $E_{\theta}[V]$ denoting the expected value of the random variable V with respect to the probability mass function $p_x(\theta)$ along these probability paths. The Fisher information enters the geodesic equation for $\theta = \theta(\xi)$. Finally, upon integrating the geodesic equation, we find the most favorable time parametrizations of γ_{θ} and, consequently, the optimum cooling paths $\{p_{\text{optimum}}(\theta)\}$.

Before starting our geodesic analysis, we recall for completeness that the trajectories connecting two quantum states $|A\rangle$ and $|B\rangle$ generated by an optimal-speed unitary evolution U can be regarded as geodesic curves on the Bloch sphere. From a geometric standpoint, these unitary operators $\{U\}$ can be described by means of rotations of the Bloch sphere around the axis that is orthogonal to the hemispherical plane containing the origin along with $|A\rangle$ and $|B\rangle$ [47]. In our paper, instead, optimality means minimum entropy production and not time-optimality. In addition, minimum entropy production

probability paths are geodesic paths on the parametric manifold with elements specified by the parameter θ and not on the Bloch sphere of pure quantum states.

I. Constant $\omega_{\mathcal{H}}$

The first driving scheme that we consider is characterized by a constant $\omega_{\mathcal{H}}^{(1)}(t) = \Gamma$. In this case, the space of probability distributions $\{p(\theta)\}$ with $p(\theta) \stackrel{\text{def}}{=} [p_w(\theta), p_{w_{\perp}}(\theta)]$ is specified by the success and failure probabilities

$$p_w(\theta) \stackrel{\text{def}}{=} \sin^2 \left(\frac{\Gamma}{\hbar} \theta \right) \text{ and } p_{w_{\perp}}(\theta) \stackrel{\text{def}}{=} \cos^2 \left(\frac{\Gamma}{\hbar} \theta \right), \quad (39)$$

respectively. The probabilities in Eq. (39) present a periodic oscillatory behavior with period $T \stackrel{\text{def}}{=} (\pi\hbar)/\Gamma$ while the Fisher information $g(\theta)$ assumes the constant value $g_0 \stackrel{\text{def}}{=} (2\Gamma/\hbar)^2$. Finally, the geodesic equations yielding the most favorable time parametrizations of γ_{θ} becomes

$$\frac{d^2\theta}{d\xi^2} + \frac{1}{2g} \frac{dg}{d\theta} \left(\frac{d\theta}{d\xi} \right)^2 = 0. \quad (40)$$

Given that $g(\theta) = g_0$ together with supposing nonvanishing positive initial conditions $\theta(\xi_0) = \theta_0$ and $\dot{\theta}(\xi_0) = \dot{\theta}_0$, integration of the geodesic equation leads to the following optimum paths:

$$\theta(\xi) = \theta_0 + \dot{\theta}_0(\xi - \xi_0). \quad (41)$$

From the expression of the optimum paths in Eq. (41), we can evaluate $\mathcal{C}_{\mathcal{M}_s}$ in Eq. (13), v_E in Eq. (19), r_E in Eq. (20), and η_E in Eq. (27). Specifically, we get

$$\begin{aligned} \mathcal{C}_{\mathcal{M}_s}(\tau) &= \frac{\Gamma}{\hbar} (\tau + \tau_0 - 2\xi_0) \dot{\theta}_0, \quad v_E(\Gamma) \\ &= \frac{2\Gamma}{\hbar} \dot{\theta}_0, \text{ and } r_E(\Gamma) = \left(\frac{2\Gamma}{\hbar} \right)^2 \dot{\theta}_0^2. \end{aligned} \quad (42)$$

From Eq. (42), we observe that $v_E(\Gamma) \propto \Gamma$, $r_E(\Gamma) \propto \Gamma^2$, and $\mathcal{C}_{\mathcal{M}_s}(\tau)$ grows linearly in time with $d\mathcal{C}_{\mathcal{M}_s}/d\tau \propto v_E = r_E^{1/2}$. It is transparent from Eq. (42) that $\omega_{\mathcal{H}}^{(1)}(t) = \Gamma$, the modulus of the complex transverse field that specifies the $\text{su}(2; \mathbb{C})$ driving Hamiltonian, is the parameter to be tuned to find a suitable tradeoff between speed and efficiency (or, speed and information geometric complexity) within our analysis of quantum mechanical evolutions. For clarity, we emphasize that the expression of r_E in Eq. (42) can be obtained either from Eq. (20) or Eq. (23). In particular, we point out that the rate of entropy production inherits the typical initial-state dependence of the entropy production [48] as evident from its expression in Eq. (42). These last two clarifications apply to all quantum driving scenarios that we study here. Moreover, we remark that the linear growth with respect to the temporal variable τ of the IGC is not completely unexpected. Indeed, in all cases being considered here, there is only one control parameter θ and, roughly speaking, the explored parametric volumes reduce to explored lengths. Finally, since the motion is geodesic, the covariant acceleration vanishes and the evolution of the control parameter occurs with constant entropic speed. For this reason, to compare the various driving schemes

using the IGC, the quantity that gains more relevance is the rate of change $d\mathcal{C}_{\mathcal{M}_s}/d\tau$ of the IGCs with respect to τ .

2. Oscillating $\omega_{\mathcal{H}}$

The second driving scheme that we study is specified by $\omega_{\mathcal{H}}^{(2)}(t) = \Gamma \cos(\lambda t)$ with $\lambda \in \mathbb{R}_+$ being a frequency parameter. In this case, the space of probability distributions $\{p(\theta)\}$ with $p(\theta) \stackrel{\text{def}}{=} [p_w(\theta), p_{w_\perp}(\theta)]$ is given by

$$p_w(\theta) \stackrel{\text{def}}{=} \sin^2 \left[\frac{\Gamma}{\hbar\lambda} \sin(\lambda\theta) \right] \text{ and } p_{w_\perp}(\theta) \stackrel{\text{def}}{=} \cos^2 \left[\frac{\Gamma}{\hbar\lambda} \sin(\lambda\theta) \right], \quad (43)$$

respectively. The probabilities $p_w(\theta)$ and $p_{w_\perp}(\theta)$ exhibit a periodic oscillatory behavior with period given by $T \stackrel{\text{def}}{=} \pi/\lambda$. Furthermore, since $p_w(\theta)$ reaches its maximum value $\sin^2[\Gamma/(\hbar\lambda)]$ at $t^* \stackrel{\text{def}}{=} \pi/(2\lambda)$, we must impose the constraint $\Gamma/\lambda = h/4$ in order for $p_w(\theta)$ to reach one as its maximum value. From Eq. (43), we get $g(\theta) = (2\Gamma/\hbar)^2 \cos^2(\lambda\theta)$ while the geodesic equation becomes

$$\frac{d^2\theta}{d\xi^2} - \lambda \tan(\lambda\theta) \left(\frac{d\theta}{d\xi} \right)^2 = 0. \quad (44)$$

Remaining in the working assumptions of nonvanishing positive initial conditions $\theta(\xi_0) = \theta_0$ and $\dot{\theta}(\xi_0) = \dot{\theta}_0$, integration of the geodesic equation leads to optimum paths $\theta(\xi)$ of the form

$$\theta(\xi) = \frac{1}{\lambda} \sin^{-1}[\lambda \cos(\lambda\theta_0)(\xi - \xi_0)\dot{\theta}_0 + \sin(\lambda\theta_0)]. \quad (45)$$

As pointed out earlier, from the optimum paths in Eq. (45), we can evaluate $\mathcal{C}_{\mathcal{M}_s}$ in Eq. (13), v_E in Eq. (19), r_E in Eq. (20), and η_E in Eq. (27). We obtain

$$\begin{aligned} \mathcal{C}_{\mathcal{M}_s}(\tau) &= \frac{\Gamma}{\hbar}(\tau + \tau_0 - 2\xi_0)\dot{\theta}_0 |\cos(\lambda\theta_0)|, \quad v_E(\Gamma) \\ &= \frac{2\Gamma}{\hbar} |\cos(\lambda\theta_0)| \dot{\theta}_0, \text{ and } r_E(\Gamma) \\ &= \left(\frac{2\Gamma}{\hbar} \right)^2 \cos^2(\lambda\theta_0) \dot{\theta}_0^2, \end{aligned} \quad (46)$$

where $\lambda = \lambda(\Gamma) \stackrel{\text{def}}{=} (4\Gamma)/h$. From Eqs. (46) and (42), we notice that the IGC keeps growing linearly in time with $d\mathcal{C}_{\mathcal{M}_s}/d\tau \propto v_E = r_E^{1/2}$. The geodesic motion, however, yields cooler optimum paths that are explored with a smaller entropic speed.

3. Power law decay of $\omega_{\mathcal{H}}$

The third driving scheme is characterized by $\omega_{\mathcal{H}}^{(3)}(t) = \Gamma/(1 + \lambda t)^2$. In this case, the space of probability distributions $\{p(\theta)\}$ is given by $p(\theta) \stackrel{\text{def}}{=} [p_w(\theta), p_{w_\perp}(\theta)]$ with

$$p_w(\theta) \stackrel{\text{def}}{=} \sin^2 \left[\frac{\Gamma}{\hbar\lambda} \left(1 - \frac{1}{1 + \lambda\theta} \right) \right] \text{ and } p_{w_\perp}(\theta) \stackrel{\text{def}}{=} \cos^2 \left[\frac{\Gamma}{\hbar\lambda} \left(1 - \frac{1}{1 + \lambda\theta} \right) \right], \quad (47)$$

respectively. Provided that $\Gamma/\lambda = h/4$, $p_w(\theta)$ in Eq. (47) exhibits an asymptotic monotonic convergence to one. Moreover, the Fisher information is given by $g(\theta) = (2\Gamma/\hbar)^2(1 + \lambda\theta)^{-4}$ while the geodesic equation is

$$\frac{d^2\theta}{d\xi^2} - \frac{2\lambda}{1 + \lambda\theta} \left(\frac{d\theta}{d\xi} \right)^2 = 0. \quad (48)$$

As previously mentioned, we keep assuming nonvanishing positive initial conditions $\theta(\xi_0) = \theta_0$ and $\dot{\theta}(\xi_0) = \dot{\theta}_0$. Then, integrating the geodesic equation, we obtain the optimum paths given by

$$\theta(\xi) = \frac{(1 + \lambda\theta_0)^2 + \lambda\dot{\theta}_0 \left[(\xi - \xi_0) - \frac{1 + \lambda\theta_0}{\lambda\dot{\theta}_0} \right]}{\lambda^2 \dot{\theta}_0 \left[\frac{1 + \lambda\theta_0}{\lambda\dot{\theta}_0} - (\xi - \xi_0) \right]}. \quad (49)$$

From the optimum paths in Eq. (49), we compute $\mathcal{C}_{\mathcal{M}_s}$ in Eq. (13), v_E in Eq. (19), r_E in Eq. (20), and η_E in Eq. (27). In particular, we get

$$\begin{aligned} \mathcal{C}_{\mathcal{M}_s}(\tau) &= \frac{\Gamma}{\hbar}(\tau + \tau_0 - 2\xi_0)\dot{\theta}_0 \frac{1}{[1 + \lambda(\Gamma)\theta_0]^2}, \quad v_E(\Gamma) \\ &= \frac{2\Gamma}{\hbar} \frac{1}{[1 + \lambda(\Gamma)\theta_0]^2} \dot{\theta}_0, \text{ and } r_E(\Gamma) \\ &= \left(\frac{2\Gamma}{\hbar} \right)^2 \frac{1}{[1 + \lambda(\Gamma)\theta_0]^4} \dot{\theta}_0^2, \end{aligned} \quad (50)$$

with $\lambda(\Gamma) \stackrel{\text{def}}{=} (4\Gamma)/h$. Analogous to the first and second scenarios, the motion on the manifold associated with the third scenario proceeds at constant entropic speed v_E and, thus, exhibits minimum entropy production. The IGC keeps growing linearly in time with $d\mathcal{C}_{\mathcal{M}_s}/d\tau \propto v_E = r_E^{1/2}$. In particular, this third scenario is characterized by a geodesic motion that gives rise to optimum paths that are cooler than those corresponding to the second scenario.

4. Exponential decay of $\omega_{\mathcal{H}}$

The fourth driving scheme is characterized by $\omega_{\mathcal{H}}^{(4)}(t) = \Gamma e^{-\lambda t}$. In this case, the space of probability distributions $\{p(\theta)\}$ is given by $p(\theta) \stackrel{\text{def}}{=} [p_w(\theta), p_{w_\perp}(\theta)]$, where

$$p_w(\theta) \stackrel{\text{def}}{=} \sin^2 \left[\frac{\Gamma}{\hbar\lambda} (1 - e^{-\lambda\theta}) \right] \text{ and } p_{w_\perp}(\theta) \stackrel{\text{def}}{=} \cos^2 \left[\frac{\Gamma}{\hbar\lambda} (1 - e^{-\lambda\theta}) \right], \quad (51)$$

respectively. We note that as long as $\Gamma/\lambda = h/4$, the probability $p_w(\theta)$ in Eq. (51) presents an asymptotic monotonic convergence to one. Employing Eq. (51), the Fisher information becomes $g(\theta) = (2\Gamma/\hbar)^2 e^{-2\lambda\theta}$ and the geodesic equation is

$$\frac{d^2\theta}{d\xi^2} - \lambda \left(\frac{d\theta}{d\xi} \right)^2 = 0. \quad (52)$$

Integrating the geodesic equation and assuming a set of nonvanishing positive initial conditions $\theta(\xi_0) = \theta_0$ and $\dot{\theta}(\xi_0) = \dot{\theta}_0$, the optimum paths become

$$\theta(\xi) = \theta_0 - \frac{1}{\lambda} \log[1 - \lambda\dot{\theta}_0(\xi - \xi_0)]. \quad (53)$$

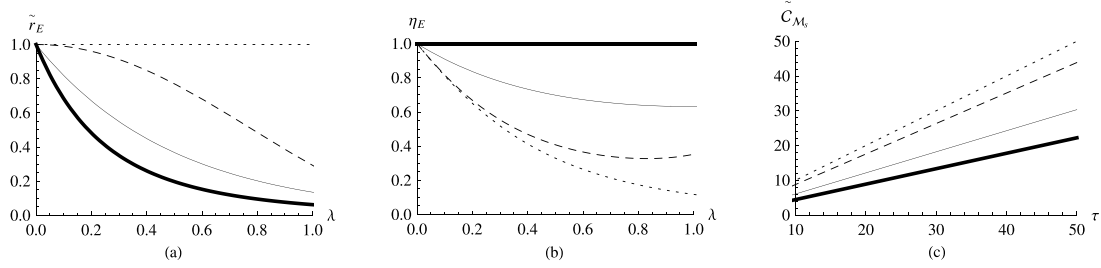


FIG. 1. We plot in panel (a) the rescaled entropy production rate \tilde{r}_E versus λ , the parameter that characterizes the field intensity. In panel (b), we depict the behavior of the entropic efficiency η_E versus λ . In panel (c), we plot $\tilde{C}_{\mathcal{M}_s}$ versus τ with $\tilde{C}_{\mathcal{M}_s}$ being the rescaled version of the information geometric complexity $\mathcal{C}_{\mathcal{M}_s}$ in its long-time limit. In panels (a), (b), and (c), the dotted, dashed, thin solid, and thick solid lines correspond to the constant, oscillatory, exponential law decay, and power law decay field intensity behaviors, respectively. Finally, we set $\theta_0 = 1$ in all plots and $\lambda = 1/2$ in panel (c).

From the optimum paths in Eq. (53), we calculate $\mathcal{C}_{\mathcal{M}_s}$ in Eq. (13), v_E in Eq. (19), r_E in Eq. (20), and η_E in Eq. (27). In particular, we obtain

$$\begin{aligned} \mathcal{C}_{\mathcal{M}_s}(\tau) &= \frac{\Gamma}{\hbar}(\tau + \tau_0 - 2\xi_0)\dot{\theta}_0 e^{-\lambda\theta_0}, v_E(\Gamma) \\ &= \frac{2\Gamma}{\hbar}e^{-\lambda(\Gamma)\theta_0}\dot{\theta}_0, \text{ and } r_E(\Gamma) = \left(\frac{2\Gamma}{\hbar}\right)^2 e^{-2\lambda(\Gamma)\theta_0}\dot{\theta}_0^2, \end{aligned} \quad (54)$$

where $\lambda(\Gamma) \stackrel{\text{def}}{=} (4\Gamma)/h$. We observe that the IGC grows linearly in time with $d\mathcal{C}_{\mathcal{M}_s}/d\tau \propto v_E = r_E^{1/2}$. In Fig. 1, we compare the four driving schemes for relatively small values of λ . We have three plots in Fig. 1. In plot (a), we represent the rescaled entropy production rate \tilde{r}_E with $r_E = (2\Gamma/\hbar)^2\dot{\theta}_0^2\tilde{r}_E$ as a function of λ . In plot (b), we depict the behavior of the entropic efficiency η_E versus λ . In plot (c), we represent the behavior of $\tilde{C}_{\mathcal{M}_s}$ versus τ . The quantity $\tilde{C}_{\mathcal{M}_s}$ denotes the rescaled version of the information geometric complexity $\mathcal{C}_{\mathcal{M}_s}$ in its long-time limit with $\mathcal{C}_{\mathcal{M}_s}^{\text{asymptotic}} = (\Gamma/\hbar)\dot{\theta}_0\tilde{C}_{\mathcal{M}_s}$. In plots (a), (b), and (c), the dotted, dashed, thin solid, and thick solid lines correspond to the constant, oscillatory, exponential law decay, and power law decay field intensity behaviors, respectively. Finally, we set $\theta_0 = 1$ in all plots and $\lambda = 1/2$ in plot (c). Then, comparing Eqs. (50) and (54), we arrive at the conclusion that for values of λ sufficiently large this fourth scenario yields the coolest optimum paths that are explored at the slowest entropic speed. In particular, when $\theta_0 \in \mathbb{R}_+$ and $\lambda(\Gamma) \stackrel{\text{def}}{=} (4\Gamma)/h \gg 1$, the following chain of inequalities hold true:

$$0 \leq e^{-\lambda\theta_0} \leq 1/(1 + \lambda\theta_0)^2 \leq |\cos(\lambda\theta_0)| \leq 1. \quad (55)$$

Therefore, for values of the parameter λ sufficiently large, the power law decay strategy outruns the exponential decay strategy in terms of entropic speed. To estimate numerically a typical value of λ from a physics standpoint, we recall that $\lambda = (4\Gamma)/h$, $\Gamma = (|e\hbar B_\perp|)/2mc$, and thus, $\lambda = (1/\pi)(|e|/mc) B_\perp$. Therefore, for a magnetic field with intensity B_\perp of the order of 0.1 T (a half of a value typical of neodymium magnets), $\lambda \approx 18$ [MKSA]. Interestingly, there are parametric regions specified by smaller values of λ (for instance, $0 \leq \lambda \lesssim 1$), where the exponential-decay strategy can outperform the power-law strategy in terms of entropic speed.

However, its performance declines in terms of either higher information geometric complexity or lower entropic efficiency. In Fig. 2, we have three plots. In plot (a), we depict the entropy production rate r_E versus λ and set $\theta_0 = 1$. The thin solid and thick solid lines denote the exponential law and the power law decay scenarios, respectively. The intersection between the two lines occurs at $\lambda \simeq 2.51$. In plot (b), we illustrate the parametric region $\mathcal{D}(\theta_0, \lambda)$ where $r_E^{(\text{exponential})}(\theta_0, \lambda) \leq r_E^{(\text{power-law})}(\theta_0, \lambda)$ (black region). Finally, in plot (c) we visualize the ratios $R_{\mathcal{C}_{\mathcal{M}_s}} \stackrel{\text{def}}{=} \mathcal{C}_{\mathcal{M}_s}^{(\text{exponential})}/\mathcal{C}_{\mathcal{M}_s}^{(\text{power-law})}$ (thick solid line) and $R_{r_E} \stackrel{\text{def}}{=} r_E^{(\text{exponential})}/r_E^{(\text{power-law})}$ (thin solid line) versus λ with θ_0 set equal to one. We emphasize that the exponential law decay scheme outperforms the power law decay scheme in terms of both entropy production rate and information geometric complexity in the limit of sufficiently large values of λ . As a final remark, we remark that in all four scenarios it happens that $d\dot{\mathcal{C}}_{\mathcal{M}_s}/dv_E = 1/2 \geq 0$ with $\dot{\mathcal{C}}_{\mathcal{M}_s} \stackrel{\text{def}}{=} d\mathcal{C}_{\mathcal{M}_s}/d\tau$. Moreover, setting the efficiency η_E in Eq. (27) equal to $\eta_E(r_{\min}, r_E)$ with $r_E = v_E^2$, we have

$$\frac{d\eta_E}{dv_E} = -\frac{4r_{\min}v_E}{(r_{\min} + v_E^2)^2} \leq 0. \quad (56)$$

Therefore, the entropic efficiency η_E is a monotonic decreasing function of the entropic speed v_E while the temporal rate of change of the information geometric complexity $\dot{\mathcal{C}}_{\mathcal{M}_s}$ is a monotonic increasing function of v_E with $d\eta_E/dv_E \leq 0$ and $d\dot{\mathcal{C}}_{\mathcal{M}_s}/dv_E \geq 0$, respectively. A summary of the relative ranking among the driving schemes considered appears in Table I.

VI. CONCLUDING REMARKS

We present here a summary of our main findings along with possible future directions.

A. Summary of results

We provided an information geometric description of quantum driving schemes specified by $\text{su}(2; \mathbb{C})$ time-dependent Hamiltonians [see Eq. (31)] in terms of both complexity [see Eq. (13)] and efficiency [see Eq. (27)] concepts. Specifically, starting from the parametrized pure output quantum states $\{|\psi(\theta)\rangle\}$ describing the evolution of a spin-1/2 particle in an external time-dependent magnetic field, we considered

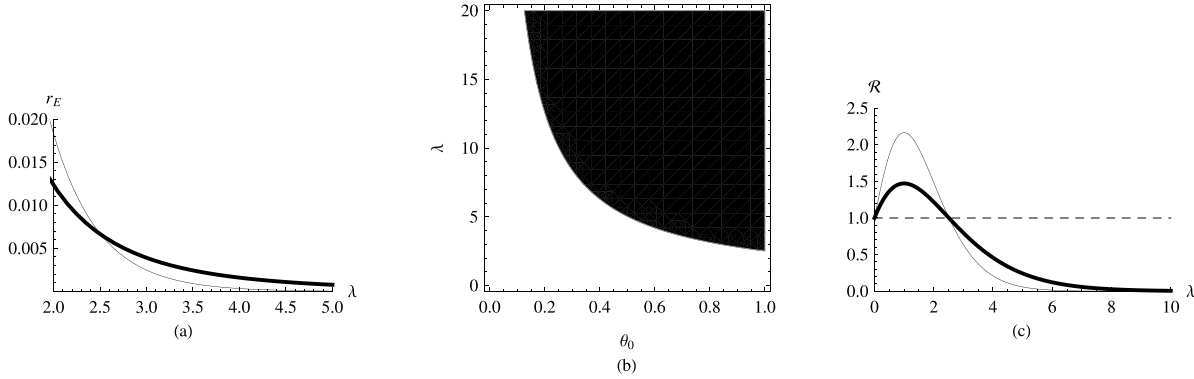


FIG. 2. In panel (a), we plot the entropy production rate r_E versus λ and set $\theta_0 = 1$. The thin solid and thick solid lines represent the exponential law and the power law decay scenarios, respectively. The intersection between the two lines occurs at $\lambda \simeq 2.51$. In panel (b), we plot the parametric region $\mathcal{D}(\theta_0, \lambda)$ where $r_E^{(\text{exponential})}(\theta_0, \lambda) \leq r_E^{(\text{power-law})}(\theta_0, \lambda)$ (black region). Finally, in panel (c) we plot the ratios $R_{\mathcal{C}_{\mathcal{M}_s}} \stackrel{\text{def}}{=} \mathcal{C}_{\mathcal{M}_s}^{(\text{exponential})} / \mathcal{C}_{\mathcal{M}_s}^{(\text{power-law})}$ (thick solid line) and $R_{r_E} \stackrel{\text{def}}{=} r_E^{(\text{exponential})} / r_E^{(\text{power-law})}$ (thin solid line) versus λ with θ_0 set equal to one. We note that the exponential law decay scheme outperforms the power law decay scheme in terms of both entropy production rate and information geometric complexity in the limit of sufficiently large values of λ .

the probability paths $\{p(\theta)\}$ emerging from the parametrized squared probability amplitudes of quantum origin with θ denoting statistical parameter corresponding to the elapsed time. The information manifold \mathcal{M}_s of such paths was equipped with a Riemannian metrization specified by the Fisher information $g_{\alpha\beta}(\theta)$ evaluated along the parametrized squared probability amplitudes. Employing a minimum action principle, the optimum path connecting initial and final states on the manifold in finite time tuned out to be the geodesic path between the two states. In particular, the total entropy production that occurs during the transfer is minimized along these optimum paths [see Eqs. (41), (45), (49), and (53)]. For each optimum path that emerges from the given quantum driving scheme, we evaluated [see Eqs. (42), (46), (50), and (54)] the IGCs, the entropic speeds, and the rates of entropy production used to define our entropic efficiency measure in Eq. (27). From our analytical estimates of complexity and efficiency, we provided a relative ranking among the driving schemes being investigated (see Fig. 1, Fig. 2, and Table I).

The following points are of particular interest:

[i] We established a link between the IGC and the thermodynamic length. Specifically, the IGC can be regarded as a measure of the “average” maximal number of statistically distinguishable states along the path γ_θ since we have $\mathcal{C}_{\mathcal{M}_s}(\tau) = \langle \mathcal{L}(\xi) \rangle_{\tau_0 \leq \xi \leq \tau}$. The validity of this equation holds for the models we have investigated here. We do not expect this relation to hold in its neat form in higher-dimensional

parameter spaces where, for instance, the equality between $ds \stackrel{\text{def}}{=} [g_{\alpha\beta}(\theta)d\theta^\alpha d\theta^\beta]^{1/2}$ and $d\mathcal{V} \stackrel{\text{def}}{=} [g(\theta)]^{1/2} d^n\theta$ with $\theta = (\theta^1, \dots, \theta^n)$ does not hold anymore. After all, $\mathcal{C}_{\mathcal{M}_s}$ is related to volume elements $d\mathcal{V}$ while \mathcal{L} is a length emerging from the integration of infinitesimal line elements ds .

[ii] We brought to light that the IGC of a geodesic path is connected to the entropy production rate along that path. In particular, the rate of change in time of the IGC is proportional to the square-root of the entropy production rate along the path γ_θ where $\theta = \theta(\xi)$ with $\tau_0 \leq \xi \leq \tau$, $d\mathcal{C}_{\mathcal{M}_s}/d\tau \propto r_E^{1/2}$, with the constant of proportionality being equal to 1/2. The validity of this relation holds for the models we considered. It would be interesting to explore what happens in more complicated scenarios with a richer Hamiltonian dynamics with more tunable parameters.

[iii] We determined that the entropic efficiency η_E is a monotonic decreasing function of the entropic speed v_E while the temporal rate of change of the information geometric complexity $\dot{\mathcal{C}}_{\mathcal{M}_s} \stackrel{\text{def}}{=} d\mathcal{C}_{\mathcal{M}_s}/d\tau$ is a monotonic increasing function of v_E with $d\eta_E/dv_E \leq 0$ and $d\dot{\mathcal{C}}_{\mathcal{M}_s}/dv_E \geq 0$. Therefore, for the driving schemes being considered here, higher speed values yield less efficient and more complex probability paths. This is a manifestation of the so-called speed-efficiency trade-off along with the conjecture, at this stage, that efficiency demands simplicity: Less (complex) is more (efficient). A major achievement would be that of constructing a driving

TABLE I. Schematic description of the entropy production rate r_E , the entropic efficiency η_E , and the information geometric complexity $\mathcal{C}_{\mathcal{M}_s}$ in the four $\text{su}(2; \mathbb{C})$ Hamiltonian being considered. In the limit of sufficiently large values of the parameter λ used to modify the behavior of the external driving field, both higher efficiency and lower complexity levels appear to be reached in the case of the driving scheme specified by an exponential law decay.

Hamiltonian model	Rate of entropy production	Efficiency	Complexity
B_\perp , constant	higher	lower	higher
B_\perp , oscillating	high	low	high
B_\perp , power law decay	low	high	low
B_\perp , exponential law decay	lower	higher	lower

scheme that is simultaneously fast, efficient, and as simple as possible according to the laws of physics. We believe the work presented here will help us pursue this goal in future efforts.

B. Outlook

Our work can be improved in a number of ways. One of the main restrictions of our investigation is its limitation to a single control parameter. However, we believe our analysis can be extended to more than one control variable in a relatively straightforward manner. Furthermore, our information geometric analysis focuses on pure states and unitary evolution. In particular, we have ignored considering more realistic scenarios where the quantum system is open to the environment and dissipation effects in the form of dynamical fluctuations of the controlled system (which, in general, is described by a mixed quantum state) become important. In general, the temporal rate of change of the density operator of an open quantum system can be expressed in terms of the sum of two terms, the Hamiltonian piece and the dissipative piece [49]. In a sense, the information geometric techniques we used here can be regarded as applied to a closed quantum system viewed as an open quantum system in the limit in which the dissipative piece is zero and the rate of change of the density operator is solely expressed in terms of the Hamiltonian piece. For a recent nongeometric study on the dynamics of a two-level system which interacts with a dissipative bosonic environment at zero temperature specified by a Lorentzian spectral density function, we refer to Ref. [50]. Moving from unitary evolution of pure states to open systems described by impure states, a number of challenges emerge. For instance, for pure states undergoing unitary dynamics, the Fisher information metric is essentially the unique contractive Riemannian metric that can be defined to quantify the distance between states [51,52]. However, there is no unique suitable metric for characterizing the distance between mixed states describing quantum systems open to the environment. Furthermore, quantifying in an analytical manner minimum dissipation protocols in the presence of a large number of experimentally tunable parameters is rather challenging from a computational standpoint, in both classical and quantum scenarios. For a numerically intensive investigation of nontrivial minimum dissipation protocols for nanomagnetic (classical) spin models in the presence of a large number of control parameters, we refer to Ref. [36]. The extension of our proposed information geometric analysis to the case of a dissipative dynamics of an open quantum system interacting with an external environment in the presence of a large number of tunable parameters can represent a number of additional challenges. They will be the subject of forthcoming investigations.

In conclusion, despite its limitations, we believe that the analysis presented here is a relevant piece of work that joins the increasing list of recent investigations concerning an information geometric characterization of entropy production and efficiency in both classical and quantum systems [9–12] and deserves further investigation.

ACKNOWLEDGMENTS

C.C. is grateful to the United States Air Force Research Laboratory (AFRL) Summer Faculty Fellowship Program for

providing support for this work. S.R. acknowledges support from the National Research Council Research Associate Fellowship program (NRC-RAP). P.M.A. acknowledges support from the Air Force Office of Scientific Research (AFOSR). Any opinions, findings and conclusions or recommendations expressed in this material are those of the author(s) and do not necessarily reflect the views of the Air Force Research Laboratory (AFRL). The Authors thank the anonymous Referees for stimulating comments leading to an improved version of the manuscript.

APPENDIX A: EQUIVALENCE OF GEODESIC EQUATIONS

In this Appendix, motivated by Eq. (18) in Sec. III, we show that the geodesic equations emerging from considering the variations $\delta(\int \sqrt{ds^2})$ and $\delta(\int ds^2) \stackrel{\text{def}}{=} g_{\alpha\beta}(\theta)d\theta^\alpha d\theta^\beta$,

$$\frac{d^2\theta^\rho}{d\xi^2} + \Gamma_{\mu\nu}^\rho \frac{d\theta^\mu}{d\xi} \frac{d\theta^\nu}{d\xi} = 0, \quad (\text{A1})$$

and

$$\frac{d}{d\xi} \left(g_{\mu\rho} \frac{d\theta^\mu}{d\xi} \right) - \frac{1}{2} \frac{d\theta^\mu}{d\xi} \frac{\partial g_{\mu\nu}}{\partial \xi^\rho} \frac{d\theta^\nu}{d\xi} = 0, \quad (\text{A2})$$

respectively, are equivalent. Indeed, using standard tensor algebra techniques, observe that

$$\begin{aligned} 0 &= \frac{d}{d\xi} \left(g_{\mu\rho} \frac{d\theta^\mu}{d\xi} \right) - \frac{1}{2} \frac{d\theta^\mu}{d\xi} \frac{\partial g_{\mu\nu}}{\partial \theta^\rho} \frac{d\theta^\nu}{d\xi} \\ &= \frac{d}{d\xi} (g_{\mu\rho}) \frac{d\theta^\mu}{d\xi} + g_{\mu\rho} \frac{d^2\theta^\mu}{d\xi^2} - \frac{1}{2} \frac{\partial g_{\mu\nu}}{\partial \theta^\rho} \frac{d\theta^\mu}{d\xi} \frac{d\theta^\nu}{d\xi} \\ &= \frac{\partial g_{\mu\rho}}{\partial \theta^\nu} \frac{d\theta^\nu}{d\xi} \frac{d\theta^\mu}{d\xi} + g_{\mu\rho} \frac{d^2\theta^\mu}{d\xi^2} - \frac{1}{2} \frac{\partial g_{\mu\nu}}{\partial \theta^\rho} \frac{d\theta^\mu}{d\xi} \frac{d\theta^\nu}{d\xi} \\ &= \frac{1}{2} \left(\frac{\partial g_{\mu\rho}}{\partial \theta^\nu} + \frac{\partial g_{\nu\rho}}{\partial \theta^\mu} \right) \frac{d\theta^\mu}{d\xi} \frac{d\theta^\nu}{d\xi} \\ &\quad + g_{\mu\rho} \frac{d^2\theta^\mu}{d\xi^2} - \frac{1}{2} \frac{\partial g_{\mu\nu}}{\partial \theta^\rho} \frac{d\theta^\mu}{d\xi} \frac{d\theta^\nu}{d\xi} \\ &= g_{\mu\rho} \frac{d^2\theta^\mu}{d\xi^2} + \frac{1}{2} \left(\frac{\partial g_{\mu\rho}}{\partial \theta^\nu} + \frac{\partial g_{\nu\rho}}{\partial \theta^\mu} - \frac{\partial g_{\mu\nu}}{\partial \theta^\rho} \right) \frac{d\theta^\mu}{d\xi} \frac{d\theta^\nu}{d\xi} \\ &= g_{\mu\rho} \frac{d^2\theta^\mu}{d\xi^2} + \Gamma_{\rho,\mu\nu} \frac{d\theta^\mu}{d\xi} \frac{d\theta^\nu}{d\xi} \\ &= g^{\rho\rho} g_{\mu\rho} \frac{d^2\theta^\mu}{d\xi^2} + g^{\rho\rho} \Gamma_{\rho,\mu\nu} \frac{d\theta^\mu}{d\xi} \frac{d\theta^\nu}{d\xi} \\ &= \frac{d^2\theta^\rho}{d\xi^2} + \Gamma_{\mu\nu}^\rho \frac{d\theta^\mu}{d\xi} \frac{d\theta^\nu}{d\xi}. \end{aligned} \quad (\text{A3})$$

Therefore, we conclude that Eqs. (A1) and (A2) are equivalent.

APPENDIX B: PHYSICAL SIGNIFICANCE OF ENTROPY PRODUCTION RATE

In this Appendix, we discuss the physical significance of the concept of entropy production rate in Eq. (20) of Sec. III in relation to the thermodynamics of a system of spin-1/2 particles driven by an external magnetic field.

1. Negative temperature of a spin-1/2 particle in an external magnetic field

In statistical physics, phenomena of negative temperatures have much less practical importance than phenomena of positive temperatures. However, negative temperatures are characteristic of atomic systems with inverted populations, and they can be equally well-described from a thermodynamical standpoint. In particular, if the entropy σ of a system is not a monotonically increasing function of its internal energy U , then it exhibits a negative temperature whenever $1/T \stackrel{\text{def}}{=} (\partial\sigma/\partial U)_X$ is negative with X standing for all the other extensive variables the entropy might depend upon [53]. More generally, the three essential requirements for a thermodynamical system to be capable of negative temperature are [54]: (i) To describe the system in terms of the concept of temperature, the elements of the system must be in thermodynamical equilibrium among themselves; (ii) there must be an upper bound to the values of the energy of the allowed states of the system; (iii) the system must be thermally isolated from all systems which do not fulfill conditions (i) and (ii). A simple physical example of a system for which a negative temperature emerges is given by a spin-1/2 particles in an external magnetic field with only two energy states available to each element of the system. Let us assume that the energies of the upper and lower states are given by $\epsilon_2 \stackrel{\text{def}}{=} +\epsilon$ and $\epsilon_1 \stackrel{\text{def}}{=} -\epsilon$, respectively, so that the energy gap between the two energy levels is $\Delta\epsilon \stackrel{\text{def}}{=} \epsilon_2 - \epsilon_1 = 2\epsilon > 0$. Furthermore, let us denote with p_{ϵ_2} and p_{ϵ_1} the probabilities of occupying the upper and lower states, respectively, with $p_{\epsilon_2} + p_{\epsilon_1} = 1$. Making use of the canonical ensemble formalism in statistical mechanics, setting the Boltzmann constant k_B equal to one, and recalling that the entropy of the system is the logarithm of the number of accessible states, it happens that $\sigma(U)$ can be recast as

$$\sigma(U) = - \left[\frac{N\epsilon_2 - U}{N\Delta\epsilon} \log \left(\frac{N\epsilon_2 - U}{N\Delta\epsilon} \right) + \frac{U - N\epsilon_1}{N\Delta\epsilon} \log \left(\frac{U - N\epsilon_1}{N\Delta\epsilon} \right) \right], \quad (\text{B1})$$

where $-N\epsilon \leq U \stackrel{\text{def}}{=} \sum_i p_{\epsilon_i} \epsilon_i = \langle E \rangle \leq N\epsilon$ is the average energy of the system, with N denoting the total number of elements of the system. The region of negative slope of this curve $\sigma(U)$ in Eq. (B1) corresponds to negative temperature. When the lowest possible energy state is fully occupied, we have $p_{\epsilon_1} = 1$, $U = -N\epsilon$, and the state is a highly ordered state at $+0^\circ\text{K}$ with $\sigma = 0$. When the highest possible energy state is fully occupied, instead, we have $p_{\epsilon_2} = 1$, $U = +N\epsilon$, and the state is a highly ordered state at -0°K with $\sigma = 0$. The states at $\pm 0^\circ\text{K}$ are completely different from a physics standpoint. When the system is at $+0^\circ\text{K}$, it cannot become colder since it cannot give up its energy anymore. When the system is at -0°K , instead, it cannot become hotter since it cannot absorb energy anymore. We remark that a system in a negative temperature state is very hot and gives up energy to any system at positive temperature put into contact with it. Negative temperatures correspond to higher energies than positive temperatures. Furthermore, unlike what happens for positive temperatures, an increased internal energy corresponds to

diminished entropy at negative temperatures. At intermediate energies with $-N\epsilon < U < N\epsilon$, when some elements are in the low-energy state and others in the high-energy state, there is greater entropy since there is less order. Therefore, between the lowest and the highest energy states of the thermodynamic system, the entropy passes through a maximum and then diminishes with increasing U . The maximum (with $\sigma_{\text{max}} = \log 2$) occurs at $U = 0$ where $p_{\epsilon_1} = p_{\epsilon_2} = 1/2$. Right before and after $U = 0$, $T = +\infty^\circ\text{K}$ and $T = -\infty^\circ\text{K}$, respectively. This change of sign in the temperature is a consequence of the inversion of the population levels with $p_{\epsilon_2}/p_{\epsilon_1} = e^{-\beta\Delta\epsilon} > 1$ when $0 < U < +N\epsilon$ with $\beta \stackrel{\text{def}}{=} (k_B T)^{-1}$. For a discussion on experimental realizations of negative temperatures with systems of interacting nuclear spins, we refer to Refs. [55,56].

2. Physical interpretation of the rate of entropy production

In what follows, we provide a more physical interpretation of the rate of entropy production given by

$$r_E \stackrel{\text{def}}{=} \frac{d}{d\tau} \mathcal{I}(\tau) = \frac{d}{d\tau} \left[\int_0^\tau \frac{d\theta^\alpha}{d\xi} g_{\alpha\beta}(\theta) \frac{d\theta^\beta}{d\xi} d\xi \right], \quad (\text{B2})$$

where $\mathcal{I}(\tau)$ is the *thermodynamic divergence*, by exploiting our thermodynamic considerations concerning negative temperature spin-1/2 systems in external magnetic fields with entropy given as in Eq. (B1).

For a physical system in equilibrium with a large thermal reservoir, it happens that the thermodynamic metric tensor $g_{\alpha\beta}[\theta(\xi)]$ in Eq. (B2) represents the covariance matrix of fluctuations around equilibrium,

$$\overline{\delta X_{\alpha\beta}^2} \stackrel{\text{def}}{=} \langle (X_\alpha - \langle X_\alpha \rangle)(X_\beta - \langle X_\beta \rangle) \rangle, \quad (\text{B3})$$

with $\{X_\alpha(x)\}$ being the thermodynamic variables that specify the Hamiltonian of the system while $\{x\}$ are the configuration space variables. Moreover, $\{\theta^\alpha\}$ are the experimentally controllable parameters of the system and $\langle \cdot \rangle$ denotes the ensemble average with respect to the canonical Gibbs distribution function $p(x|\theta) \equiv p_x(\theta) = e^{-\theta^\alpha(\xi)X_\alpha(x)}/\mathcal{Z}$ with \mathcal{Z} being the partition function of the system. After some straightforward algebra, it can be shown that the thermodynamic metric tensor and the Fisher-Rao information metric tensor are equivalent. Specifically, we have

$$g_{\alpha\beta}(\theta) = \overline{\delta X_{\alpha\beta}^2} = \sum_x p_x(\theta) \frac{\partial \log p_x(\theta)}{\partial \theta^\alpha} \frac{\partial \log p_x(\theta)}{\partial \theta^\beta}. \quad (\text{B4})$$

Using Eq. (B4), r_E in Eq. (B2) can be recast as

$$r_E = \frac{d\theta^\alpha}{d\xi} \overline{\delta X_{\alpha\beta}^2} \frac{d\theta^\beta}{d\xi} = \sum_x p_x(\theta) \left(\frac{d \log p_x(\theta)}{d\xi} \right)^2, \quad (\text{B5})$$

with $\theta = \theta(\xi) \stackrel{\text{def}}{=} [\theta^1(\xi), \dots, \theta^n(\xi)]$ with n being the dimensionality of the parameter space. From Eqs. (B4) and (B5), we point out that while the Fisher-Rao information metric tensor is defined in terms of *partial* derivatives of the probabilities with respect to the control parameters, the rate of entropy production is specified by *total* derivative of the probabilities $\frac{dp_x(\theta)}{d\xi} = \frac{\partial p_x(\theta)}{\partial \theta^\alpha} \frac{d\theta^\alpha}{d\xi}$, with respect to the affine parameter ξ along the trajectories $\{\theta^\alpha(\xi)\}$. For a *single* control parameter

$\theta^\alpha(\xi) \rightarrow \theta(\xi)$ the above two formulas Eqs. (B4) and (B5) are deceptively similar,

$$g_{\alpha\beta}(\theta) \rightarrow g(\theta) = \sum_x p_x(\theta) \left(\frac{\partial \log p_x(\theta)}{\partial \theta} \right)^2, \\ r_E \rightarrow \sum_x p_x(\theta) \left(\frac{d \log p_x(\theta)}{d\xi} \right)^2, \quad (\text{B6})$$

differing only in the use of type of derivative employed to differentiate the ‘‘score function’’ $\log p_x(\theta)$. Moreover, from Eq. (B5), we observe that r_E can be also described as the ‘‘product’’ of the fluctuation term $\overline{\delta X}_{\alpha\beta}^2$ and the square of the total rate of change with respect to the affine parameter ξ of the control parameter $\theta^\alpha(\xi)$.

To better grasp the significance of the rate of entropy production, we consider the following illustrative comparison. First, we consider a system with probability path defined by $p(\theta) \stackrel{\text{def}}{=} [p_{\epsilon_1}(\theta), p_{\epsilon_2}(\theta)] = [\sin^2(\theta), \cos^2(\theta)]$ with $\theta(\xi) = (\pi/2)\xi$ and $0 \leq \xi \leq 1$. In this first case, we obtain $r_E = \pi^2$. This system exhibits features that are similar to those characterizing a two-level system as transparent from the link between the probabilities defining $p(\theta) \stackrel{\text{def}}{=} [p_w(\theta), p_{w_\perp}(\theta)] \rightarrow p(\beta) \stackrel{\text{def}}{=} [p_{\epsilon_1}(\beta), p_{\epsilon_2}(\beta)]$. Here, as in Crooks [28,57], we use the variable inverse temperature $\beta(\xi) = [k_B T(\xi)]^{-1}$ as the single control parameter θ . For the canonical ensemble we have $p_{\epsilon_1}(\beta) \stackrel{\text{def}}{=} e^{-\beta\epsilon_1}/\mathcal{Z} = e^{-(\beta\epsilon_1 + \log \mathcal{Z})}$ with $\mathcal{Z} \stackrel{\text{def}}{=} e^{-\beta\epsilon_1} + e^{-\beta\epsilon_2}$. Noting that $\frac{\partial \log p_{\epsilon_1}}{\partial \beta} = \bar{\epsilon} - \epsilon_1$, with $\bar{\epsilon} \stackrel{\text{def}}{=} \sum_i p_{\epsilon_i}(\beta)\epsilon_i$ we see that the Fisher information in Eq. (B6) becomes $g(\theta) = \overline{\delta E}^2 \stackrel{\text{def}}{=} \sum_i p_{\epsilon_i}(\beta)(\epsilon_i - \bar{\epsilon})^2$, the variance of the energy fluctuations. Inserting this into the expression for r_E in Eq. (B5), and using $\frac{dp_x(\theta)}{d\xi} = \frac{\partial p_x(\theta)}{\partial \beta} \frac{d\beta}{d\xi}$, we find that the entropy production rate r_E is the product of the energy fluctuations $\overline{\delta E}^2$ times the squared rate of change $(\frac{d\beta}{d\xi})^2$ of the control parameter along the trajectory in parameter space

$$r_E = \overline{\delta E}^2 \left(\frac{d\beta}{d\xi} \right)^2 = \left(\frac{dp_{\epsilon_1}}{d\xi} \right)^2 \left(\frac{1}{p_{\epsilon_1}} + \frac{1}{p_{\epsilon_2}} \right) = \pi^2. \quad (\text{B7})$$

Note that the second equality in Eq. (B7) arises (after a little algebra) from comparing the two terms in the first equality, respectively, to functions of the probabilities. Equation (B7) is in agreement with the calculation of the rate of entropy production carried out in the first case. Moreover, we remark that the quantity $dp_{\epsilon_1}/d\xi$, which acts as a kind of ‘‘probability velocity’’ for the two-level system along the trajectory in parameter space, can be regarded as a relative energy fluctuation term since $dp_{\epsilon_1}/d\xi \propto \overline{\delta E}/\epsilon$ while the term $(1/p_{\epsilon_1} + 1/p_{\epsilon_2})$ (which, we note, can be viewed as the reciprocal of a reduced probability mass term) is proportional to the square of the rate of change of the control parameter β with respect to the affine time parameter ξ , $(1/p_{\epsilon_1} + 1/p_{\epsilon_2}) \propto (d\beta/d\xi)^2$. Thus, the form of Eq. (B7) is reminiscent of a kind of ‘‘kinetic energy of fluctuations’’ of the two-level system along the trajectory in parameter space. As a side remark, we refer to Ref. [58] for an interesting link between the Fisher information function in information geometry and the concept of entropic acceleration in thermodynamics. Finally, for further details on negative

temperatures and fluctuations in thermodynamics, we refer to Ref. [53].

APPENDIX C: PRESERVING THE RELATIVE RANKING

In this Appendix, we check that the relative ranking of the driving schemes provided by the three distinct measures of entropic efficiency introduced in Sec. III is preserved.

Recall that the three efficiency measures $\eta_E^{(1)}(r_E)$, $\eta_E^{(2)}(r_E)$, and $\eta_E(r_E^{(l)}, r_E^{(m)})$ are defined as

$$\eta_E^{(1)}(r_E) \stackrel{\text{def}}{=} 1 - \frac{r_E}{r_E^{\max}}, \quad \eta_E^{(2)}(r_E) \stackrel{\text{def}}{=} \frac{r_E^{\min}}{r_E}, \quad \text{and} \quad \eta_E(r_E^{(l)}, r_E^{(m)}) \\ \stackrel{\text{def}}{=} 1 - \frac{|r_E^{(l)} - r_E^{(m)}|}{r_E^{(l)} + r_E^{(m)}}, \quad (\text{C1})$$

respectively. If we assume that $r_E^{(i_*)} \geq r_E^{(i'_*)}$, then a straightforward calculation yields

$$\eta_E^{(1)}(r_E^{(i_*)}) \leq \eta_E^{(1)}(r_E^{(i'_*)}), \quad \eta_E^{(2)}(r_E^{(i_*)}) \leq \eta_E^{(2)}(r_E^{(i'_*)}), \quad \text{and} \\ \eta_E(r_E^{(i_*)}, r_E^{\min}) \leq \eta_E(r_E^{(i'_*)}, r_E^{\min}). \quad (\text{C2})$$

Similarly, when $r_E^{(i_*)} \leq r_E^{(i'_*)}$, we get

$$\eta_E^{(1)}(r_E^{(i_*)}) \geq \eta_E^{(1)}(r_E^{(i'_*)}), \quad \eta_E^{(2)}(r_E^{(i_*)}) \geq \eta_E^{(2)}(r_E^{(i'_*)}), \quad \text{and} \\ \eta_E(r_E^{(i_*)}, r_E^{\min}) \geq \eta_E(r_E^{(i'_*)}, r_E^{\min}). \quad (\text{C3})$$

Note that i_* and i'_* are arbitrary indices with $1 \leq i_*, i'_* \leq \bar{N}$ with \bar{N} being the number of different driving schemes being ranked. Therefore, given the arbitrariness of the inequalities $r_E^{(i_*)} \geq r_E^{(i'_*)}$ and $r_E^{(i_*)} \leq r_E^{(i'_*)}$, we conclude from Eqs. (C2) and (C3) that $\eta_E^{(1)}(r_E)$, $\eta_E^{(2)}(r_E)$, and $\eta_E(r_E^{(l)}, r_E^{(m)})$ rank the driving schemes in a similar manner by preserving the relative order from the best one to the worst one.

APPENDIX D: PARAMETRIZATION OF PROBABILITY AMPLITUDES

In this Appendix, we report a general parametrization of the probability amplitudes $\alpha(t)$ and $\beta(t)$ that appear in Eq. (36) of Sec. IV.

Following Refs. [17,18], it happens that $\alpha(t)$ and $\beta(t)$ in Eq. (36) can be recast as

$$\begin{cases} \alpha(t) = \{\cos[\Phi(t)] - i \frac{b}{\sqrt{1+b^2}} \sin[\Phi(t)]\} e^{i \frac{\phi_\omega(t)}{2}}, \\ \beta(t) = \frac{1}{\sqrt{1+b^2}} \sin[\Phi(t)] e^{i[\frac{\phi_\omega(t)}{2} - \frac{\pi}{2}]}, \end{cases} \quad (\text{D1})$$

with $\Phi(t)$ defined as $\Phi(t) \stackrel{\text{def}}{=} \sqrt{1+b^2} \int_0^t \frac{|\omega(t')|}{\hbar} dt'$, provided that $\Omega(t) + \hbar \dot{\phi}_\omega(t)/2 = b|\omega(t)|$ where b is an arbitrary real number/parameter. Clearly, $|\omega(t)|$ is the magnitude of the complex transverse field $\omega(t) = |\omega(t)|e^{i\phi_\omega(t)}$ with $|\omega(t)| \propto B_\perp(t)$ and $\Omega(t)$ is the real longitudinal field with $|\Omega(t)| \propto B_\parallel(t)$. In particular, the resonance regime is specified by $b \rightarrow 0$ with $\alpha(t)$ and $\beta(t)$ in Eq. (D1) reducing to

$$\begin{cases} \alpha(t) = \cos \left[\int_0^t \frac{|\omega(t')|}{\hbar} dt' \right] e^{i \frac{\phi_\omega(t)}{2}}, \\ \beta(t) = \sin \left[\int_0^t \frac{|\omega(t')|}{\hbar} dt' \right] e^{i[\frac{\phi_\omega(t)}{2} - \frac{\pi}{2}]}. \end{cases} \quad (\text{D2})$$

For more details, we refer to the original work in Refs. [17,18].

- [1] L. Kronsjö, *Algorithms: Their Complexity and Efficiency* (John Wiley & Sons Ltd., New York, NY, 1987).
- [2] A. Montanaro, Quantum algorithms: An overview, *npj Quantum Info.* **2**, 15023 (2016).
- [3] M. A. Nielsen and I. L. Chuang, *Quantum Computation and Quantum Information* (Cambridge University Press, Cambridge, UK, 2000).
- [4] C. Cafaro and S. Mancini, A geometric algebra perspective on quantum computational gates and universality in quantum computing, *Adv. Appl. Clifford Alg.* **21**, 493 (2011).
- [5] H. T. Kung and J. F. Traub, Computational complexity of one-point and multi-point iteration, in *Complexity of Real Computation*, edited by R. Karp (American Mathematical Society, Providence, RI, 1973).
- [6] S. Amari and H. Nagaoka, *Methods of Information Geometry* (Oxford University Press, Oxford, UK, 2000).
- [7] G. Ruppeiner, Riemannian geometry in thermodynamic fluctuation theory, *Rev. Mod. Phys.* **67**, 605 (1995).
- [8] G. Ruppeiner, Erratum: Riemannian geometry in thermodynamic fluctuation theory, *Rev. Mod. Phys.* **68**, 313 (1996).
- [9] T. Van Vu and Y. Hasegawa, Geometrical Bounds of the Irreversibility in Markovian Systems, *Phys. Rev. Lett.* **126**, 010601 (2021).
- [10] H. J. D. Miller and M. Mehboudi, Geometry of work Fluctuations Versus Efficiency in Microscopic Thermal Machines, *Phys. Rev. Lett.* **125**, 260602 (2020).
- [11] K. Brandner and K. Saito, Thermodynamic Geometry of Microscopic Heat Engines, *Phys. Rev. Lett.* **124**, 040602 (2020).
- [12] S. Ito, M. Oizumi, and S. Amari, Unified framework for the entropy production and the stochastic interaction based on information geometry, *Phys. Rev. Res.* **2**, 033048 (2020).
- [13] C. Cafaro and P. M. Alsing, Decrease of Fisher information and the information geometry of evolution equations for quantum mechanical probability amplitudes, *Phys. Rev. E* **97**, 042110 (2018).
- [14] C. Cafaro and P. M. Alsing, Information geometry aspects of minimum entropy production paths from quantum mechanical evolutions, *Phys. Rev. E* **101**, 022110 (2020).
- [15] S. Gassner, C. Cafaro, S. A. Ali, and P. M. Alsing, Information geometric aspects of probability paths with minimum entropy production for quantum state evolution, *Int. J. Geom. Methods Mod. Phys.* **18**, 2150127 (2021).
- [16] C. Cafaro and P. M. Alsing, Continuous-time quantum search and time-dependent two-level quantum systems, *Int. J. Quantum. Inform.* **17**, 1950025 (2019).
- [17] A. Messina and H. Nakazato, Analytically solvable Hamiltonians for quantum two-level systems and their dynamics, *J. Phys. A: Math. Theor.* **47**, 445302 (2014).
- [18] R. Grimaudo, A. S. M. de Castro, H. Nakazato, and A. Messina, Classes of exactly solvable generalized semi-classical Rabi systems, *Ann. Phys.* **530**, 1800198 (2018).
- [19] D. Castelvecchi, Clash of the physics laws, *Nature (London)* **543**, 597 (2017).
- [20] S. L. Braunstein, C. M. Caves, and G. J. Milburn, Generalized uncertainty relations: Theory, examples, and Lorentz invariance, *Ann. Phys.* **247**, 135 (1996).
- [21] C. Cafaro and S. A. Ali, Jacobi fields on statistical manifolds of negative curvature, *Physica D* **234**, 70 (2007).
- [22] C. Cafaro, The information geometry of chaos, Ph.D. thesis, State University of New York at Albany, NY, 2008, [arXiv:1601.07935](https://arxiv.org/abs/1601.07935) [math-ph].
- [23] S. A. Ali, C. Cafaro, S. Gassner, and A. Giffin, An information geometric perspective on the complexity of macroscopic predictions arising from incomplete information, *Adv. Math. Phys.* **2018**, 2048521 (2018).
- [24] S. A. Ali, C. Cafaro, D.-H. Kim, and S. Mancini, The effect of microscopic correlations on the information geometric complexity of Gaussian statistical models, *Physica A* **389**, 3117 (2010).
- [25] D. Felice, C. Cafaro, and S. Mancini, Information geometric methods for complexity, *Chaos* **28**, 032101 (2018).
- [26] S. A. Ali and C. Cafaro, Theoretical investigations of an information geometric approach to complexity, *Rev. Math. Phys.* **29**, 1730002 (2017).
- [27] C. Cafaro, A. Giffin, S. A. Ali, and D.-H. Kim, Reexamination of an information geometric construction of entropic indicators of complexity, *Appl. Math. Comput.* **217**, 2944 (2010).
- [28] G. E. Crooks, Measuring thermodynamic length, *Phys. Rev. Lett.* **99**, 100602 (2007).
- [29] G. Ruppeiner, Thermodynamics: A Riemannian geometric model, *Phys. Rev. A* **20**, 1608 (1979).
- [30] F. Weinhold, Metric geometry of equilibrium thermodynamics, *J. Chem. Phys.* **63**, 2479 (1975).
- [31] P. Salamon and R. S. Berry, Thermodynamic Length and Dissipated Availability, *Phys. Rev. Lett.* **51**, 1127 (1983).
- [32] T. Feldmann, B. Andresen, A. Qi, and P. Salamon, Thermodynamic lengths and intrinsic time scales in molecular relaxation, *J. Chem. Phys.* **83**, 5849 (1985).
- [33] W. K. Wootters, Statistical distance and Hilbert space, *Phys. Rev. D* **23**, 357 (1981).
- [34] L. Diosi, G. Forgacs, B. Lukacs, and H. L. Frisch, Metricization of thermodynamic-state space and the renormalization group, *Phys. Rev. A* **29**, 3343 (1984).
- [35] L. Diosi, K. Kulacsy, B. Lukacs, and A. Racz, Thermodynamic length, time, speed, and optimum path to minimize entropy production, *J. Chem. Phys.* **105**, 11220 (1996).
- [36] G. M. Rostskoff, G. E. Crooks, and E. Vanden-Eijnden, Geometric approach to optimal nonequilibrium control: Minimizing dissipation in nanomagnetic spin systems, *Phys. Rev. E* **95**, 012148 (2017).
- [37] B. Andresen and J. M. Gordon, Constant thermodynamic speed for minimizing entropy production in thermodynamic processes and simulated annealing, *Phys. Rev. E* **50**, 4346 (1994).
- [38] W. Spirkel and H. Ries, Optimal finite-time endoreversible processes, *Phys. Rev. E* **52**, 3485 (1995).
- [39] E. P. Gyftopoulos and G. P. Beretta, *Thermodynamics: Foundations and Applications* (Dover Publications, Mineola, NY, 2005).
- [40] J. Anandan and Y. Aharonov, Geometry of Quantum Evolution, *Phys. Rev. Lett.* **65**, 1697 (1990).
- [41] C. Cafaro, S. Ray, and P. M. Alsing, Geometric aspects of analog quantum search evolutions, *Phys. Rev. A* **102**, 052607 (2020).
- [42] R. C. Tolman and P. C. Fine, On the irreversible production of entropy, *Rev. Mod. Phys.* **20**, 51 (1948).
- [43] C. Cafaro and P. M. Alsing, Theoretical analysis of a nearly optimal analog quantum search, *Phys. Scr.* **94**, 085103 (2019).

- [44] C. Cafaro, S. Gassner, and P. M. Alsing, Information geometric perspective on off-resonance effects in driven two-level quantum systems, *Quant. Rep.* **2**, 166 (2020).
- [45] S. L. Braunstein and C. M. Caves, Statistical Distance and Geometry of Quantum States, *Phys. Rev. Lett.* **72**, 3439 (1994).
- [46] J. J. Sakurai, *Modern Quantum Mechanics* (Addison-Wesley Publishing, Boston, MA, 1994).
- [47] D. C. Brody, Elementary derivation for passage times, *J. Phys. A: Math. Gen.* **36**, 5587 (2003).
- [48] P. M. Riechers and M. Gu, Initial-state dependence of thermodynamic dissipation for any quantum process, *Phys. Rev. E* **103**, 042145 (2021).
- [49] P. Hayden and J. Sorce, On the magnitude of dissipation in open quantum systems, [arXiv:2108.08316](https://arxiv.org/abs/2108.08316) [quant-ph].
- [50] W. Wu and Z.-Z. Zhang, Controllable dynamics of a dissipative two-level system, *Sci. Rep.* **11**, 7188 (2021).
- [51] D. C. Brody and B. Longstaff, Evolution speed of open quantum dynamics, *Phys. Rev. Research* **1**, 033127 (2019).
- [52] E. O'Connor, G. Guarneri, and S. Campbell, Action quantum speed limits, *Phys. Rev. A* **103**, 022210 (2021).
- [53] C. Kittel, *Elementary Statistical Physics* (John Wiley & Sons, New York, NY, 1958).
- [54] N. Ramsey, Thermodynamics and statistical mechanics at negative absolute temperature, *Phys. Rev.* **103**, 20 (1956).
- [55] E. M. Purcell and R. V. Pound, A nuclear spin system at negative temperature, *Phys. Rev.* **81**, 279 (1951).
- [56] A. Abragam and W. G. Proctor, Experiments on spin temperature, *Phys. Rev.* **106**, 160 (1957).
- [57] G. E. Crooks, Fisher information and statistical mechanics, Technical note 008v4, <http://threeplusone.com/sher> (2012).
- [58] S. B. Nichols, A. del Campo, and J. R. Green, Nonequilibrium uncertainty principle from information geometry, *Phys. Rev. E* **98**, 032106 (2018).